



**Politecnico
di Torino**

Politecnico di Torino

Master's Degree

Biomedical Engineering - Biomechanics

Academic Year: 2022/2023

March 15th, 2023

**Carbon Dioxide Capture by Carbon Dots
as a Promising Approach to Reduce
Global Warming**

Supervisors:

Prof. Alberto Tagliaferro

Dr. Mattia Bartoli

Candidate:

Susanna Bedendo

Index

ABSTRACT	4
1. Introduction	6
1.1 CO ₂ separation methods	7
1.2 Carbon Dots	8
1.2.1 Structure and properties	8
1.2.2 Preparation techniques	10
1.2.3 CDs beyond biological applications	11
1.3 Selectivity towards CO ₂ by CDs	12
1.4 Capture methods	13
2. Materials and Methods	16
2.1 Materials	16
2.2 Synthesis processes	17
2.2.1 Synthesis of CDs for CO ₂ adsorption	17
2.2.2 Synthesis of uniform CNDs	19
2.3 Characterization methods	20
2.4 Adsorption method for CDs	21
2.5 TGA and BET techniques	22
3. Results	24
3.1 Characterization	24
3.2 CO ₂ adsorption	38
3.2.1 TGA without the dehydration step	38
3.2.2 TGA with the dehydration step	43
3.3 Comparison with the state of art	49
3.4 Uniform structure of CNDs	52
	2

4. Conclusions	58
Acknowledgements	60
References	61

ABSTRACT

Climate change is a major crisis that affects human lives with a detrimental impact on decades of progress in global health. As a major contributor to the climate change, global warming that is mainly attributed to CO₂ emission demands an effective mitigation strategy. Under such a circumstance, nanomaterials with high surface-area-to-volume ratios are promising in CO₂ capture. As a relatively new family member of carbon-based nanomaterials, carbon dots (CDs) that possess small particle sizes (1-10 nm) but high surface-area-to-volume ratios and abundant surface functional groups such as amine and hydroxyl groups are particularly favored for this application.

In this study, four types of CDs, namely carbon nitride dots, gel-like CDs, pentaethylenhexamine (PEHA)-derived CDs, and yellow-emission CDs, were synthesized by following their respective well-established protocols. They were characterized by UV/vis absorption, fluorescence emission, Fourier-transform infrared spectroscopies, and atomic force microscopy. It is noteworthy that when a controlled synthesis was conducted for carbon nitride dots, a unique fluorescence behavior was observed. Then all the CDs were tested for CO₂ adsorption capacity with the help of thermogravimetric analysis, and the CO₂ adsorption capacity of the CDs in natural state was arranged in the order of gel-CDs (67 mg/g) > PEHA-CDs (28 mg/g) > yellow-CDs (10 mg/g) and carbon nitride dots (10 mg/g). In order to accurately analyze the CO₂ adsorption capacity of gel-CDs and determine whether it is amine or hydroxyl group, that plays a dominant role in the CO₂ capture, TGA was performed on the demoinsturized, and modified gel-CDs, respectively, which showed that gel-CDs possess a high CO₂ uptake capacity of 67 mg/g that is determined by both functional groups. Subsequently, as a demonstrated photocatalyst material, gel-CDs were applied to efficiently convert CO₂ into organic matter.

In conclusion, this study reveals the structure-property relationship of CDs in CO₂ capture and conversion. Significantly, it demonstrates a great potential of CDs in the global warming reduction as well as affiliated applications in agriculture and cosmetics.

1. Introduction

Nowadays climate change is among the major crisis of our planet. It hugely impacts in human lives and health by endangering clean air, safe drinking water, nutritious food supply and environment. It has a potential to undermine decades of progress in global health. Since 2016, climate change has been declared as a major crisis. As a major component of climate change, global warming is attributed to CO₂ emissions in the atmosphere because, among all the greenhouse gases, CO₂ contributes more than 65% to global warming so it is considered the biggest responsible for greenhouse effect [1]. In April 2022, for the first time CO₂ overpassed the concentration of 420 ppm, it was the first record in the humanity history, at the beginning of the industrial revolution was just 278 ppm and the global average temperature exceeded approximately 1,2 °C of the pre-industrial level [2]. In order to reduce global warming, there is an urgent need for CO₂ reductions in the atmosphere.

Typically, techniques such as absorption, adsorption, and membrane separation have all been proposed to capture CO₂. Among them, adsorption appears to be a more promising technology due to its easy operation and low energy requirements because it can be implemented at room temperature. Thus, CO₂ adsorption is a promising approach to remove CO₂, which can be operated on a large scale for commercial purposes [2].

Recently, nanomaterials with high surface-area-to-volume ratios are promising in CO₂ capture. Among them, carbon dots (CDs) that are well characterized for properties including small particle size, abundant surface functional groups, tunable surface functionality, high photoluminescence, water solubility, morphological and chemical stability, biocompatibility and nontoxicity [3]. Nonetheless, the large surface area or high surface-area-to-volume ratio and their texture with local morphology and topology enable CDs to adsorb CO₂. Significantly, many CDs species possess primary amine groups on the surface, which benefits the CO₂ adsorption because the basic groups interact with the acidic CO₂ molecule for the strong affinity. Moreover, they can be prepared easily and have a low cost [4].

In this study, four kinds of carbon dots were synthesized: carbon nitride dots (CNDs), pentaethylenehexamine (PEHA) carbon dots (P-CDs), gel carbon dots (G-CDs) and yellow carbon dots (Y-CDs). CNDs and P-CDs were prepared from citric acid with urea and citric acid with PEHA, respectively via a one-step bottom-up microwave-mediated approach. G-CDs were synthesized using citric acid and ethylenediamine as precursors via bottom-up. Y-CDs were prepared from citric acid and phenylenediamine via bottom-up. They were applied as a model to investigate the CO₂ adsorption capacity of CDs due to their abundant amine and hydroxyl groups. CNDs, P-CDs and G-CDs were also prepared by changing the precursors ratio in the optic to study which functional group mattered more during the CO₂ uptake.

Although several methods on the preparation of CNDs have been reported, in most of the production process, CNDs suffer from inhomogeneity in size and shape limiting their impact. Therefore, another purpose of this study was to synthesize uniform CNDs using mesoporous silica particles as confining templates.

1.1 CO₂ separation methods

In this study, the analysis of different CO₂ separation techniques was crucial in order to understand which one was best suited to be used by CDs, the most common methods for separating carbon dioxide were [5]:

1. Absorption: CO₂ was removed from a gas stream by absorption in a solvent. The solvent is typically an amine, which reacts with CO₂ to form a more stable compound that could be separated from the gas stream. Absorption was commonly used in industrial processes such as natural gas processing and carbon capture.
2. Adsorption: CO₂ was removed from a gas stream by adsorption onto a solid material, typically a porous material such as activated carbon. The CO₂ molecules were attracted to the surface of the material and adhere to it. Adsorption was commonly used in applications such as gas separation and air purification. Depending on the type of adsorbent used, CO₂ could be adsorbed by either weak attraction forces such as electrostatic or van der Waals forces (physisorption) or through strong chemical bounds (chemisorption).

3. Membrane separation: CO₂ was separated from other gases by passing the gas mixture through a selective membrane. The membrane was designed to allow CO₂ to pass through while blocking other gases. Membrane separation was used in applications such as natural gas processing and carbon capture.
4. Cryogenic separation: in this method, CO₂ is separated from a gas stream by cooling the gas to very low temperatures. At low temperatures, CO₂ condensed into a liquid, which could be separated from the other gases in the mixture. Cryogenic separation was commonly used in industrial processes such as natural gas processing and air separation [6].

These were methods and physical principles used for separating CO₂. The choice of method depended on factors such as the concentration of CO₂ in the gas stream, the desired purity of the CO₂, and the specific application.

In this study, adsorption was the most suitable method because it appeared to be the most promising technology in order to uptake CO₂ from the atmosphere due to its easy operation, adsorbent reusability, absence of corrosion, applicability over a relatively range of temperature and pressure conditions, low capital investment costs, and low energy requirements [7]. Moreover, it could be operated in a large scale for commercial purposes compared with the other technologies. Other techniques, such as absorption, required a vast amount of equipment and a high cost due to the high energy consumption [2].

1.2 Carbon Dots

1.2.1 Structure and properties

CDs are a group of spherical carbon-based nanoparticles (NPs) with a diameter less than 10 nm which have a sp²/sp³ hybridized carbon core and a great variety of chemical functional groups at their surface. CDs as the latest member of the fluorescent nanomaterials family have drawn a considerable attraction in the fields of cancer therapy, bioimaging, chemical sensing and photocatalysis [8]. Due to many excellent physicochemical properties including the core-shell structure (fig.1), high photoluminescence, high biocompatibility, abundant and tunable surface functionalities and nontoxicity, CDs have been widely used in various applications where other NPs cannot be applied [9]. CDs are a green alternative of the traditional metal-based quantum

dots (QDs). CDs have high light-harvesting capability which could be used to improve the photosynthesis efficiency of plants. Moreover, CDs are one of the most promising drug nanocarriers. They are easy to synthesize with a large surface area to volume ratio which enhances the drug loading capacity for drug delivery and thanks to their excellent photoluminescence have been widely applied in sensing and bioimaging. CDs have high water-dispersity, which is beneficial for conducting homogeneous photocatalysis or partial drug delivery. CDs have attracted much attention due to their excellent properties and applications, especially the use for gene delivery. Considering the risks and concerns involved in the use of viral vectors for gene delivery *in vivo*, non-viral vectors such as CDs have gradually become an ideal alternative due to their biocompatibility and low toxicity.

Among all the properties of CDs, the most important for this study are definitely the high surface-area-to-volume ratio and the presence of abundant functional groups on their surface, such as amine groups, indispensable to uptake CO₂ from the atmosphere. Additionally, CDs can be functionalized based on the amount of the chosen precursors and this is useful to control the amount of functional group as amine groups and carboxylic groups. A nanostructure with more amine groups is more basic thus CDs with more amine group promotes the interaction with the acidic CO₂ molecule for the strong affinity.

CDs, as already written, are all organized in a core-shell structure, the core is the internal part with C hybridized sp²-sp³ disposed in graphitic layers; the shell is the external part which contains organic functional groups that determine the reactivity of the molecule. Based on the structure, CDs can be divided into three families:

1. Graphitic CDs: formed by hybridized sp² C planes. They are formed by a bottom-up approach starting with a C nanotube that is oxidized and broken up the small pieces. These small particles go on to re-stack forming CDs with different functional groups on the surface.
2. Carbon nitride dots: represent an upgrade of graphitic ones made from urea and an acid precursor through a bottom-up approach, characterized by a graphene-like structure but with outer planes made from triazines. They have more complex distribution than the previous ones because they have heteroatoms and more layers.

3. Polymeric CDs: are the most various group with different properties from the previous ones.

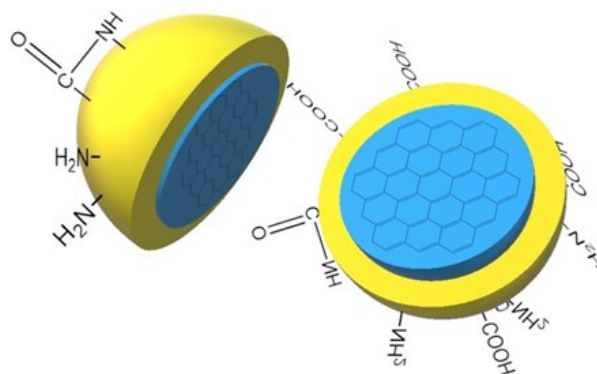


Figure 1 – Core-shell structure of CDs with functional groups on surface.

1.2.2 Preparation techniques

CDs can be prepared via two techniques: top-down and bottom-up (fig. 2) [8].

Specifically, the top-down method, a physical approach, is to achieve nanometer size, starting from a larger material, where the massive, "bulk" material is broken down into smaller particles, using mechanical, chemical or other forms of energy. This approach involves breakdown or fragmentation of larger carbon materials such as graphite, carbon soot, carbon fiber, carbon nanotube, nanodiamond into small C-dots [8]. CDs could be mainly prepared from various natural resources through this technique, including several methods such as microwave-assisted, hydrothermal, sonication process, arc-discharge, pyrolysis carbonization, chemical and electrochemical oxidation, and ultrasonic synthesis [10]. Generally top-down approaches require harsh reaction conditions, expensive materials/equipment, and long processing time [11].

By its turn, bottom-up method, a chemical approach, also called "molecular nanotechnology," is arguably the most widely used synthesis method. It refers to the synthesis of nanoparticle material through the condensation of atoms, molecules or radicals thus allowing the precursor to grow with the desired size and characteristics. This nanotechnology generally consists on the pyrolysis of smaller organic molecules either in power form (calcination) or in solution via hydrothermal or microwave-based approaches. After the thermal or combustion strategy, condensation, polymerization, carbonization and

passivation are involved in CDs formation. In the former process, small molecules or monomers come closer and form chain compounds as intermediates. They become aggregated with time and polymerized to form CDs. Depending on starting precursors, different type of functional groups are present on the surface of the CDs [8]. This “bottom-up” approach has the advantage of being suitable for mass production, being eco-friendly, and of low cost [11]. In this study, to synthesize the CDs, only the bottom-up technique was used because of its simplicity, and it allowed to have CDs a better control in the structure including particle size, shape, and distribution.

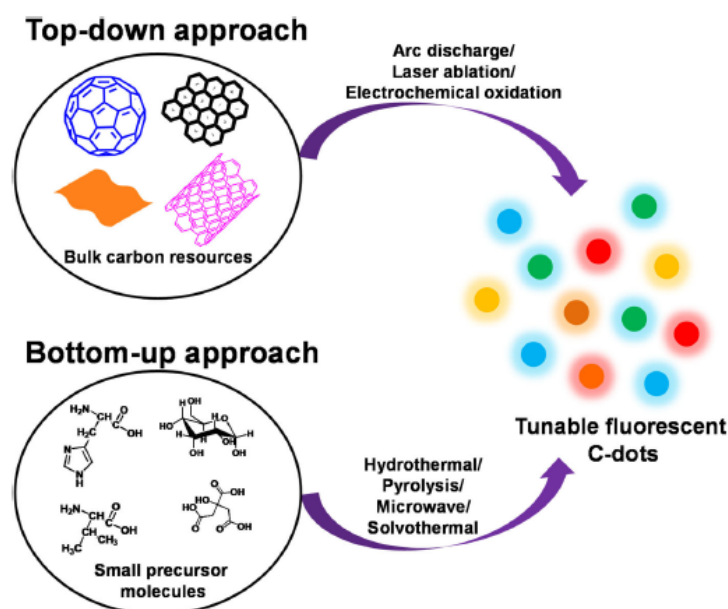


Figure 2 – General synthesis strategies to prepare CDs.

1.2.3 CDs beyond biological applications

Carbon dots have a wide range of potential applications beyond biological applications. Here are a few examples:

1. Energy storage and conversion: CDs have been shown to have excellent electrochemical properties, making them promising candidates for use in energy storage and conversion applications, such as batteries and supercapacitors [12].
2. Environmental monitoring: Carbon dots can be used as sensors to detect environmental pollutants, such as heavy metals, organic compounds, and even pathogens in water and air [13].

3. Optoelectronics: Carbon dots can be used in optoelectronic devices, such as light-emitting diodes (LEDs), solar cells, and sensors, due to their unique optical and electronic properties [14].
4. Catalysis: Carbon dots can act as catalysts in a variety of chemical reactions, including the reduction of nitro compounds and the oxidation of alcohols [15].
5. Food packaging: Carbon dots have antimicrobial properties and can be used in food packaging to extend the shelf life of food products and reduce food waste [16].
6. Nanocomposites: Carbon dots can be incorporated into polymers to create nanocomposites with improved properties, such as mechanical strength, electrical conductivity, and thermal stability [17].

Overall, the unique optical and electronic properties of carbon dots made them promising candidates for a wide range of applications in various fields beyond biology.

1.3 Selectivity towards CO₂ by CDs

A potential application of CDs is in the separation of gases, such as CO₂ from N₂, O₂ and CH₄, present in the atmosphere. CDs can act as adsorbents, which means they can attract and hold onto molecules. The separation of gases using CDs is based on the principle of selective adsorption. When a gas mixture is passed over a bed of CDs, each gas component interacts with the surface of the CDs differently based on their molecular properties.

In addition, the surface chemistry of the CDs can be modified to enhance their selectivity for CO₂. For example, functional groups such as amine or carboxyl groups can be added to the surface of the CDs to increase their affinity for CO₂.

Once the CO₂ molecules are selectively adsorbed onto the surface of the CDs, they can be desorbed by applying a temperature or pressure swing. This allows the separation of CO₂ from N₂ and CH₄ to be accomplished in a cyclic process.

Summarizing, CDs offer a promising approach for the separation of CO₂ from other gases due to their unique optical and electronic properties, as well as their tunable surface chemistry.

1.4 Capture methods

Carbon dots can entrap CO₂ through a process called physical adsorption or physisorption. Physisorption is a type of adsorption that involves weak intermolecular forces, such as van der Waals forces, hydrogen bonding, and electrostatic interactions. Carbon dots can form a large number of weak interactions with CO₂ molecules. These interactions can cause the CO₂ molecules to be attracted to and trapped within the pores and surface of the carbon dots, without any chemical reaction taking place. The specific mechanism by which CO₂ is entrapped within carbon dots can depend on several factors, such as the size and surface chemistry of the carbon dots, the size and structure of the CO₂ molecules, and the temperature and pressure of the system (fig. 3A).

In the case of amine groups, the lone pair of electrons on the nitrogen atom can form weak hydrogen bonds with the polar CO₂ molecule. This interaction can cause the CO₂ molecule to be attracted to the surface of the amine group and adsorbed onto it. The adsorption between CO₂ and hydroxyl groups can occur through several mechanisms, including hydrogen bonding, dipole-dipole interactions, and van der Waals forces. Adsorption can also occur between CO₂ and carboxylic groups. The interaction between CO₂ and carboxylic groups can occur through hydrogen bonding and van der Waals forces. The strength of all the interactions that have been mentioned will depend on the surface area of the material, the nature and number of the groups present, and the temperature and pressure conditions.

One example of a material that can undergo adsorption with CO₂ through carboxylic groups is activated carbon. Activated carbon is a porous material that is commonly used in air and water purification applications. The carboxylic groups on the activated carbon surface can interact with CO₂ through hydrogen bonding, resulting in adsorption of CO₂ on the material surface.

Overall, carbon dots can entrap CO₂ through physical adsorption, by forming weak intermolecular forces with the CO₂ molecules. This process is a key mechanism in the development of efficient and selective materials for CO₂ uptake.

A schematic diagram of interaction of CO₂ on a pure graphene plane (fig. 3 - B, C) can be used to generalize the interaction of CO₂ on CNDs because they have graphene planes and within them heteroatoms of nitrogen. Since CNDs exhibit a graphitic nanostructure,

CO₂ entrapped within the planar layers of carbons and CO₂ has a partial positive charge on carbon and two partial negative charges on oxygens, thus, when it interacts with heteroatoms, the adsorption is favored [18].

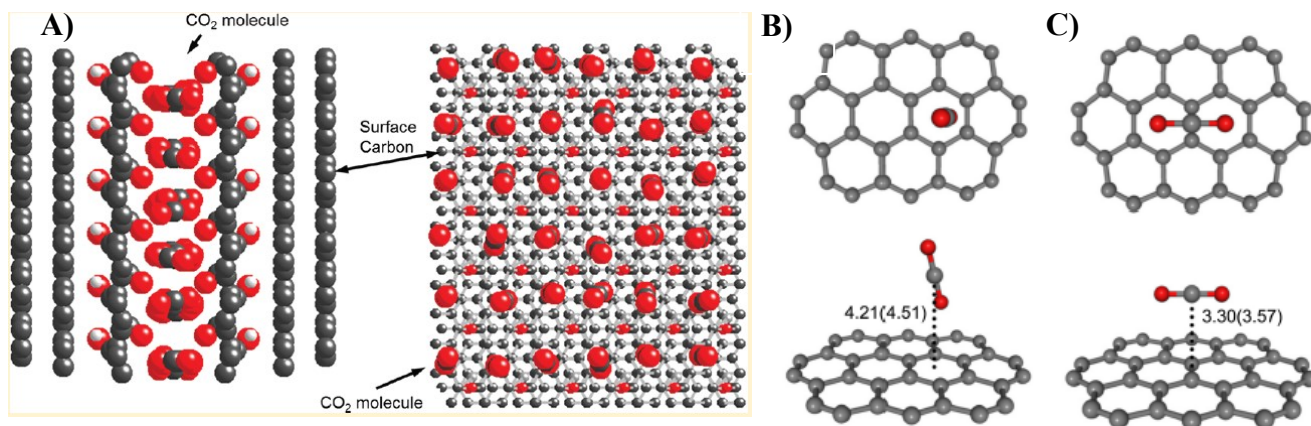


Figure 3 – A) Interaction between CO₂ and CDs. B) Interaction of CO₂ with NH₂ on a pure graphene plane. C) CO₂ is parallel to aromatic rings with delocalized bonding.

2. Materials and Methods

2.1 Materials

The precursors used for CDs were: citric acid ($\geq 98\%$), PEHA ($\geq 98\%$) and acetone (99.9%) from VWR (West Chester, PA, USA); urea, acquired from Eastman Kodak Company (Rochester, NY). For gel CDs, 1,2-ethylenediamine (EDA) ($\geq 99\%$) was provided by MP Biomedicals (Irvine, CA). For yellow CDs, 1,2-phenylenediamine (99.5%) and dimethylformamide (DMF $\geq 99.8\%$) were purchased from Sigma-Aldrich (St Louis, MO, USA) and sodium hydroxide pellets (molecular weight of 40 g/mol) was provided by Fountain Parkway (Solon, Ohio, USA). Compressed argon and nitrogen gases with ultra-high purity were acquired from Airgas (Miami, FL). The mesoporous silica particles MCM-48 (15 μm particle size, 3 nm pore size) and SBA-15 ($< 150\ \mu\text{m}$ particle size, 6 nm pore size) were purchased from Sigma-Aldrich (St Louis, MO, USA). All chemicals were used without further treatment.

The dialysis tubing with a MWCO of 100-500 Da was obtained from Spectrum Labs, Inc. (Rancho Dominguez, CA). The deionized (DI) water (resistivity: 18.2 $\text{M}\Omega\cdot\text{cm}$; surface tension: 72 $\text{mN}\cdot\text{m}^{-1}$; pH: 6.6 ± 0.3 at $20.0 \pm 0.5\ ^\circ\text{C}$) was acquired using a MilliQ3 water purification system obtained from Millipore Sigma (Burlington, MA) and used as the solvent in the preparation of CDs.

Citric acid has a molecular weight of 192.12 g/mol (1 mol = 3 mol -COOH). Urea has a molecular weight of 60.06 g/mol (1 mol = 2 mol -NH₂). PEHA has a molecular weight of 232.38 g/mol, density: 0.95 g/ml (1 mol = 2 mol -NH₂). EDA has a molecular weight of 60.1 g/mol, density: 0.9 g/ml (1 mol = 2 mol -NH₂). 1,2-phenylenediamine has a molecular weight of 108.14 g/mol (1 mol = 2 mol -NH₂). Silica has a molecular weight of 60.08 g/mol.

2.2 Synthesis processes

2.2.1 Synthesis of CDs for CO₂ adsorption

In this study, four kinds of carbon dots were synthesized: carbon nitride dots (CNDs), pentaethylenhexamine (PEHA) carbon dots (P-CDs), gel carbon dots (G-CDs) and yellow carbon dots (Y-CDs).

CNDs are an emerging carbon-based nanomaterial, it possesses rich surface functional moieties and a carbon nitride core [19]. Regarding CNDs prepared with the standard quantities of reagents, the process was the following: 0.5 g citric acid and 0.5 g urea were dissolved in 20 ml DI water and vigorously stirred overnight. Next, the mixed solution was heated in a domestic microwave oven at 700 W for 7 min. The resulting brown solid product was re-dispersed in 15 ml DI water, sonicated at 42 kHz for 60 min and centrifuged twice (5000 rpm/30 min/25 °C), so that the precipitant was removed. The supernatant was filtered (0.2 µm filter pore size) and dialyzed (MWCO: 100-500 Da) against DI water for 3 days (water was replaced every 24 h) on a stir plate to accelerate the osmosis process and remove unwanted particles. These ones had a molecular weight slower than 500 Da, selected as the cut-off dialysis membrane. Finally, the sample was kept in the freezer (-40 °C) overnight and placed into the freezer-dryer for 3 days in order to obtain a carbon nano-powder, denoted as CNDs (1:1) [20].

In this study were synthesized other kinds of CNDs but with different precursors ratios, as CNDs with 0.8 g citric acid and 0.2 g urea dissolved in 20 ml DI water, denoted as CNDs (4:1) and CNDs with 0.2 g citric acid and 0.8 g urea dissolved in 20 ml DI water, named as CNDs (1:4). The preparation process was the same as the previous one. These three kinds of CNDs will be used for analyzing the impact of surface modification on other properties of CNDs.

P-CDs were synthesized with 0.5 g citric acid and 0.5 ml PEHA are dissolved in 20 ml DI water and vigorously stirred overnight. Successively, the mixed solution was heated in a domestic microwave oven at 700 W for 7 min. The resulting brown solid product was re-dispersed in 15 ml DI water, sonicated at 42 kHz for 90 min and centrifuged once (9000 rpm/30 min/4 °C). The supernatant was filtered (0.2 µm filter pore size) and dialyzed

(MWCO: 100-500 Da) against DI water, changed every 24 h, for 3 days on a stir plate to accelerate the osmosis process and remove unwanted particles. These ones had a molecular weight slower than 500 Da, selected as the cut-off dialysis membrane. Finally, the sample was kept in the freezer (-40 °C) overnight and placed into the freezer-dryer for 3 days in order to obtain a P-CDs nano-powder, named as P-CDs (1:1) [21].

With the aim of analyzing the functional surface groups, several types of P-CDs had been synthesized besides the first: one with 0.5 g citric acid and 0.1 ml PEHA, denoted as P-CDs (5:1), another with 0.5 g citric acid and 0.8 ml PEHA, referred to as P-CDs (1:2) and the last with 0.8 g citric acid and 0.2 ml PEHA, appointed as P-CDs (4:1).

The as-prepared CNDs and PCDs were purified via centrifugation, filtration and dialysis to remove unreacted precursors and any intermediates formed during their synthesis.

To prepare gel carbon dots, first a 50-ml round-bottom flask was filled with argon gas for 5 min to expel O₂. Subsequently, 30 ml EDA was transferred to the flask and heated with constant stirring using an oil bath. When the temperature reached 160 °C, 6 g of citric acid was added to the flask. The reaction of citric acid and EDA proceeded for 50 min under the environment of argon gas for deaeration. After the solvothermal system was cooled to room temperature, the G-CDs were deposited at the bottom of the flask below the layer of unreacted EDA. To purify the G-CDs, unreacted EDA was removed with several washes with acetone. Finally 10 g of G-CDs were obtained [22].

In this study were synthesized other kinds of G-CDs but with different precursors ratios, as G-CDs with 6 g citric acid and 6 ml EDA dissolved in 20 ml DI water, denoted as G-CDs (5:1) and G-CDs with 3.75 g citric acid and 30 ml EDA dissolved in 20 ml DI water, named as G-CDs (1:2). The preparation process was the same as the previous one.

In the optic to prepare Y-CDs, 0.04 g of citric acid and 0.56 g of 1,2-phenylenediamine were used as precursors with 20 ml of DI water under nitrogen gas to protect the solution from oxidizing (about 30-45 seconds) and quickly covered with parafilm. The solution was sonicated for 1 hour until the color turned a pale yellow. Subsequently, the solution was rotavaped in a round bottom flask till to get a volume of 10 ml and a orange color due to heat. It could be considered necessary to place the solution in a ice bath for 5 minutes and sometimes it crystallized immediately. Thereafter, filtration was essential to remove

unreacted 1,2-phenylenediamine. The next step was size exclusion chromatography (SEC), cleaned three times with 0.1 M sodium hydroxide, in which the solution was filtered through. By the end, at least 200 ml of solution, with a yellow color, were obtained. To reduce the volume to 50 ml it was rotavaped again. Finally, the sample was kept in the freezer (-40 °C) overnight and placed into the freezer-dryer for 3 days in order to obtain a Y-CDs nano-powder.

2.2.2 Synthesis of uniform CNDs

The uniformity of CNDs is an important factor for a deep understanding of their structure which is fundamental to unravel the photoluminescence mechanism and their potential applications. It was expected that the uniform CDs allowed a better interpretation of different spectroscopic techniques normally used to study the chemical and physical properties of nanomaterials. Herein, this study proposed the use of nano/micro-mesoporous organic templates based on silica to obtain a more homogeneous and narrowed size distribution of CNDs; this allowed to produce a very peaked distribution of the particles. The uniformity of the nanoparticles could influence the overall properties of CNDs, especially their fluorescence properties. Therefore, uniform CNDs allowed to understand the physical and chemical characteristics of core and surface which directly influenced the CDs' properties and their final applications.

When prepared, CNDs normally presented a normal size-distribution which was statically sufficient to obtain an average size with a small standard deviation. Nevertheless, in a scenario where the structure altered with respect to the size, a normal distribution was not enough to represent the whole population. Therefore, a unique size or a narrower size-distribution could be a potential variable to be controlled during the preparation of CDs.

In order to synthesized uniform CNDs, not only was a silica template used but also a rapid heating to 500°C in few minutes. This short time was essential to have heating homogeneity and fast heat transfer.

In particular, with the optic to obtain uniform CNDs, they were prepared in a different way. Firstly, in a crucible, 0.1 g citric acid, 0.1 g urea and 0.2 g silica (pore size of 3 nm) were dissolved in 2 ml DI water and vigorously stirred. Next, the mixed solution was sonicated at 42 kHz for 15 min. Subsequently the sample was heated in the oven (95 °C)

until the solution became dry (around 3-4 h) and warmed in the autoclave for 5 min at 500 °C. This short time was essential to have heating homogeneity and fast heat transfer. Thereafter, the sample was re-dispersed in 15 ml DI water, and centrifuged twice (9000 rpm/15 min/20 °C), so that the precipitant was removed. The supernatant was filtered (0.2 µm filter pore size) and dialyzed (MWCO: 100-500 Da) against DI water for 3 days (water was replaced every 24 h) on a stir plate to accelerate the osmosis process and remove unwanted particles. These ones had a molecular weight slower than 500 Da, selected as the cut-off dialysis membrane. Finally, the sample was kept in the freezer (-40 °C) overnight and placed into the freezer-dryer for 3 days in order to obtain a carbon nano-powder. Other batches were prepared in order to obtain the most uniform CNDs, some with the use of salts: 20 mg of NaCl, 5 mg of LiCl, 5 mg of KNO₃ and with injection of pure N₂ during the heating process in the autoclave. The salts were added to template the structure of CNDs. In addition, in some solutions, silica particles with a pore size of 6 nm were used instead of the one with a pore size of 3 nm.

2.3 Characterization methods

The optical, structural and morphological properties of CDs were analyzed by using several methods: photoluminescence (PL), ultraviolet-visible spectroscopy (UV/vis), Fourier-transform infrared (FTIR) spectroscopy and atomic force (AFM). Spectroscopic techniques are based on the energy exchange that occurs between radiant energy and matter.

UV/vis spectrophotometer (Agilent Cary 100) was used to acquire UV/vis absorption spectra. Absorption spectrophotometry is based on the absorption phenomena of light radiation in the region of the electromagnetic spectrum belonging to the visible range (400 - 700 nm) and near ultraviolet (200 - 400 nm).

PL characterizations were carried out with a HORIBA Jobin Yvon Fluorolog-3 fluorometer with a slit width of 5 nm for both excitation and emission. Normalizations of PL emission spectra are achieved by using OriginPro 9.1 software. Quartz cuvettes with an optical pathlength of 1 cm were used for all the optical property characterizations. CDs are well known for their fluorescent properties.

The FTIR spectroscopy was conducted on a FTIR spectrometer (FT-Nicolet 5700, Thermo Scientific) equipped with a Smartorbit (Thermo Scientific) operation. FTIR provides information on the groups present in CDs by denoting structural features within the bulk of the CDs.

The AFM data were obtained with a 5420 atomic force microscope (Agilent Technologies) by placing a drop of CDs aqueous solution (0.1 mg/ml) on a clean silica mica slide, followed by screening in tapping mode with an applied force of 3 N/m. AFM is attained to understand the morphology and size distribution of uniform CNDs. AFM measures the particle sizes along the z-axis.

2.4 Adsorption method for CDs

As already mentioned, there were several methods that can be utilized by CDs to uptake CO₂ from the atmosphere. Among all of them, adsorption was the best method because of the following reasons:

1. high surface area: carbon dots have a high surface area, which provides a large number of active sites for CO₂ adsorption. This high surface area is due to their small size and unique surface properties, making them an ideal material for CO₂ capture.
2. selectivity: adsorption is a selective process, which means that it can separate CO₂ from other gases present in the mixture. This selectivity is due to the unique surface properties of carbon dots, which can selectively interact with CO₂ molecules.
3. regenerability: adsorption is a reversible process, which means that the adsorbed CO₂ can be easily desorbed and the carbon dots can be reused for CO₂ capture. This regenerability is an essential feature for the practical application of carbon dots in CO₂ capture.
4. cost-effective: adsorption is a cost-effective method for CO₂ capture compared to other methods such as absorption or membrane separation. The cost of materials used in adsorption, including carbon dots, is lower compared to other methods.

Overall, among all the methods, adsorption was the best candidate for CO₂ uptake due to its high surface area, selectivity, regenerability, and cost-effectiveness.

2.5 TGA and BET techniques

TGA (Thermogravimetric analysis) and BET (Brunauer–Emmett–Teller) are both techniques used to analyze the adsorption capacity of materials, including carbon dots, for gases like CO₂. TGA measures the change in weight of a material as it is exposed to different gases and temperatures, which can be used to determine the amount of gas adsorbed by the material. This allows researchers to determine the amount of CO₂ adsorbed by the sample, as well as the temperature at which the adsorption occurs, the rate of adsorption, and the stability of the adsorbed CO₂. BET, on the other hand, measures the surface area of a material by analyzing the adsorption and desorption of a gas on its surface. However, they have different strengths and limitations, and the choice of the method depends on the specific application and the properties of the material being studied.

In the case of CO₂ adsorption for carbon dots, TGA is generally considered to be a better technique than BET for determining the adsorption capacity. This is because carbon dots typically have a very small particle size, which makes it difficult to accurately measure their surface area using BET. Furthermore, TGA can provide information on the thermal stability of CDs and the nature of the interactions between the CO₂ and the surface of CDs, which can be useful in optimizing their performance as adsorbents. Another important characteristic of TGA is that allows to work both at room temperature and both at high temperatures, this feature is not common in other techniques [1].

Overall, while both techniques have their advantages and limitations, TGA is generally considered to be a more suitable technique than BET for analyzing the CO₂ adsorption capacity of carbon dots.

3. Results

3.1 Characterization

The characterizations carried out in this study can be divided into three main categories: spectroscopical (UV/visible, fluorescence and FTIR spectroscopy), morphological (AFM) and thermal (TGA).

Regarding the UV/visible spectroscopy, the radiations absorbed by molecules produce energy transitions of sigma and pi electrons. Sigma (σ) transition is the one that requires the higher amount of energy and consists of an electron cloud distributed along the bond axis. Pi (π) transition requires a lower amount of energy and it occurs between electron pairs whose density is outside the bond axis, as in double and triple bonds. $n-\pi^*$ and $n-\sigma^*$ transitions are typical of radicals, such as heteroatoms that have non-binding doublets (C=C, C=N, N=N, C-O, C-N...). A scheme of this process is showed in fig. 4.

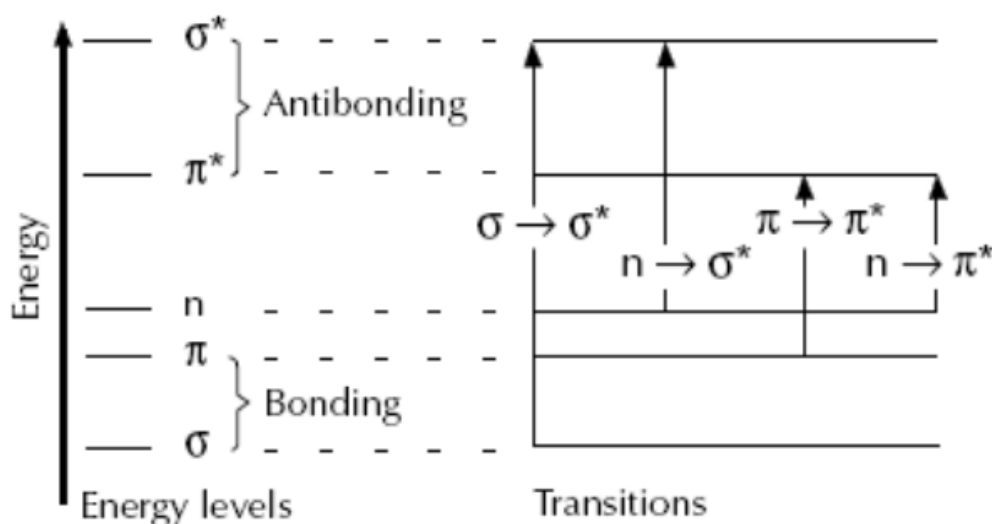


Figure 4 – Schematic diagram of transitions in chemical orbitals.

Particularly, CNDs exhibited their characteristic bands in the range of 200-400 nm. The UV/vis spectrum of CNDs (fig. 5) showed absorbance in the 200-300 nm region commonly attributed to the $\pi-\pi^*$ transition of the C=C bond and sp^2 networks as in graphene. The peaks between 300 and 400 nm were usually ascribed to the $n-\pi^*$ transition

of the C=O or C=N bond. A low energy tailing could be observed in the spectra. On the other hand, 1:4 and 4:1 CNDs presented different absorption bands. The band at 413 nm, which was assigned to $n-\pi^*$ electronic transition of C-N and C=N groups and the one at 371 nm, characteristic $n-\pi^*$ electronic transition of C=O, became more prominent for 4:1 CNDs but disappeared for 1:4 CNDs, predictable considering the increased urea amount used and thus with less carboxylic groups. Furthermore, at the wavelength of 334 nm 1:4 CNDs showed a more pronounced peak than for 4:1 CNDs, thanks to the presence of amine groups. The samples were analyzed with a concentration of 0.02 mg/ml.

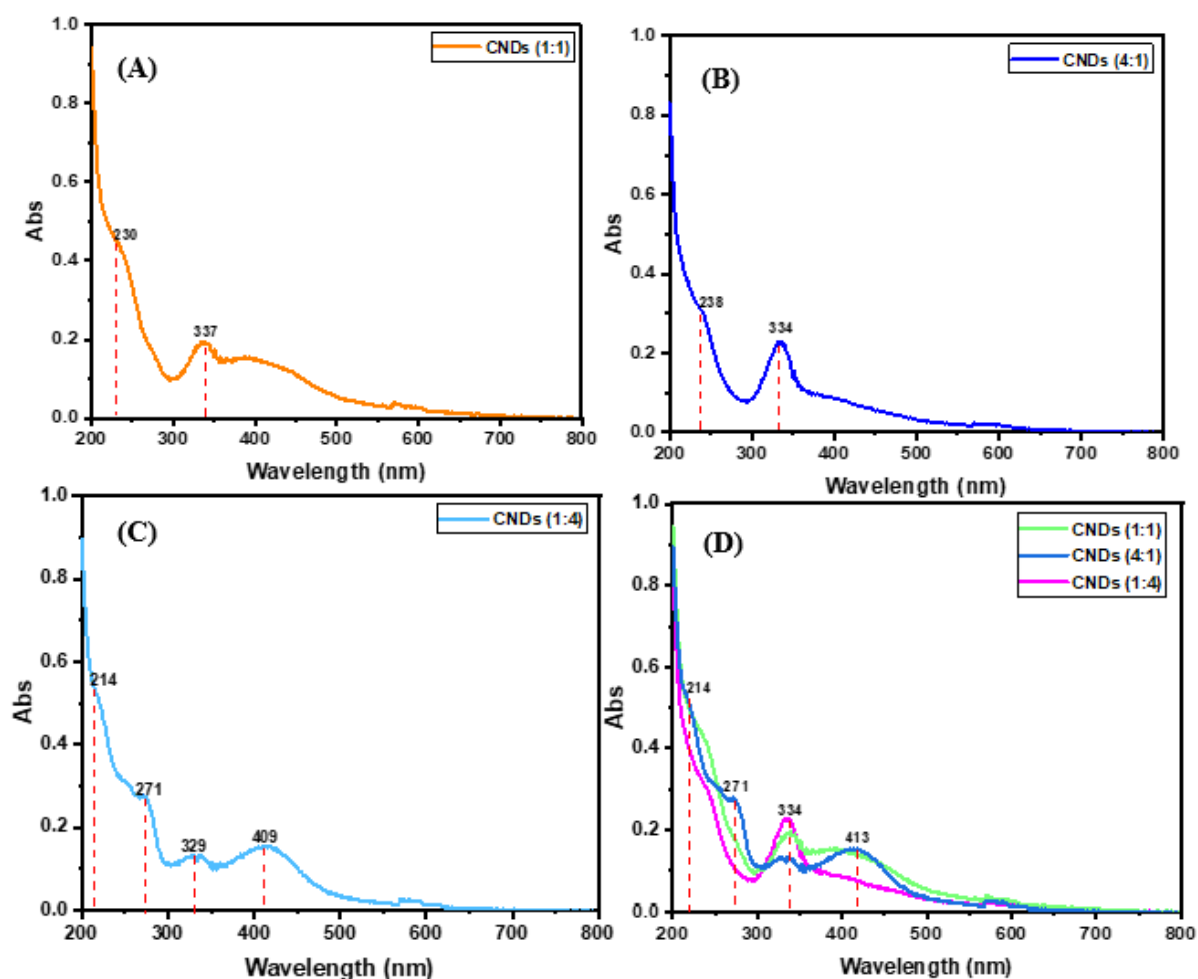
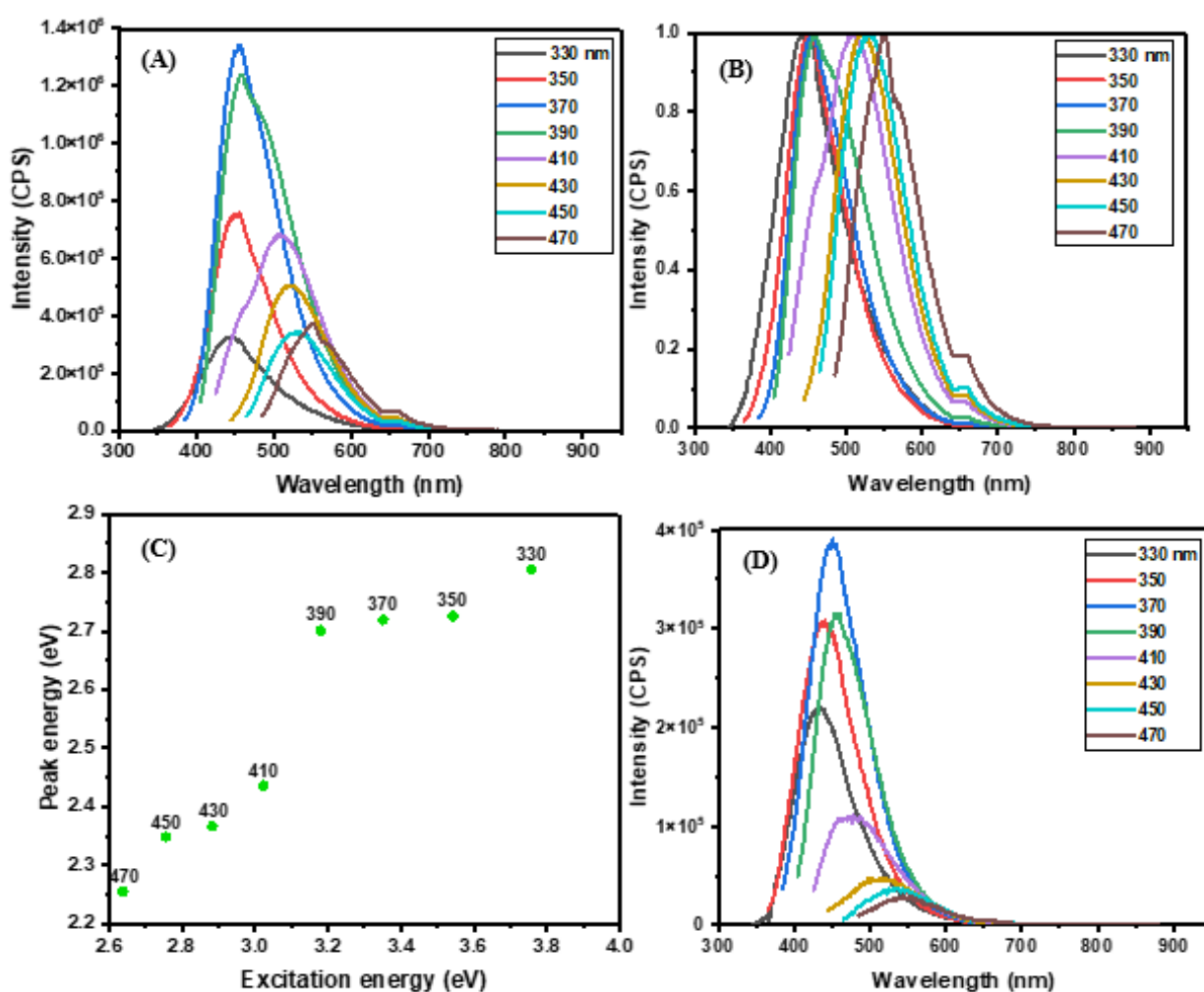


Figure 5 – **A**) UV/vis of CNDs (1:1) – **B**) UV/vis of CNDs (4:1) – **C**) UV/vis of CNDs (1:4) – **D**) UV/vis spectrum comparison between the CNDs.

In the fluorescence spectrum of CNDs, in a wavelength range of 330 nm (3.78 eV) – 470 (2.67 eV) nm the emission spectra exhibited an excitation-dependent characteristic, showed in the normalized PL spectra (fig. 6 - B, E, H), with the highest peak at 456 and 451 nm with an excitation wavelength of 370 nm for (1:1) CNDs and (4:1) CNDs,

respectively when the CNDs are excited in the $n-\pi^*$ absorption band. Instead, for (1:4) CNDs, the maximum excitation was at 518 nm with the wavelength excitation of 410 nm. By analyzing the PL emission spectra of 1:4 and 4:1 CNDs (fig. 6 - D, G), some differences could be notice comparing to 1:1 CNDs (fig. 6A). For instance, in CNDs 4:1 spectrum there was a blue-shift for the emission bands excited at 350 and 410 nm, instead in CNDs 1:4 the emission bands at 330 and 350 nm showed a blue-shift while at 370 and 390 nm a red-shift. The energy plots (fig. 6 - C, F, I) showed for all the CNDs a single peak at the excitation wavelength of 330 nm. The concentration used for all the three kinds of CNDs was 0.025 $\mu\text{g/ml}$.



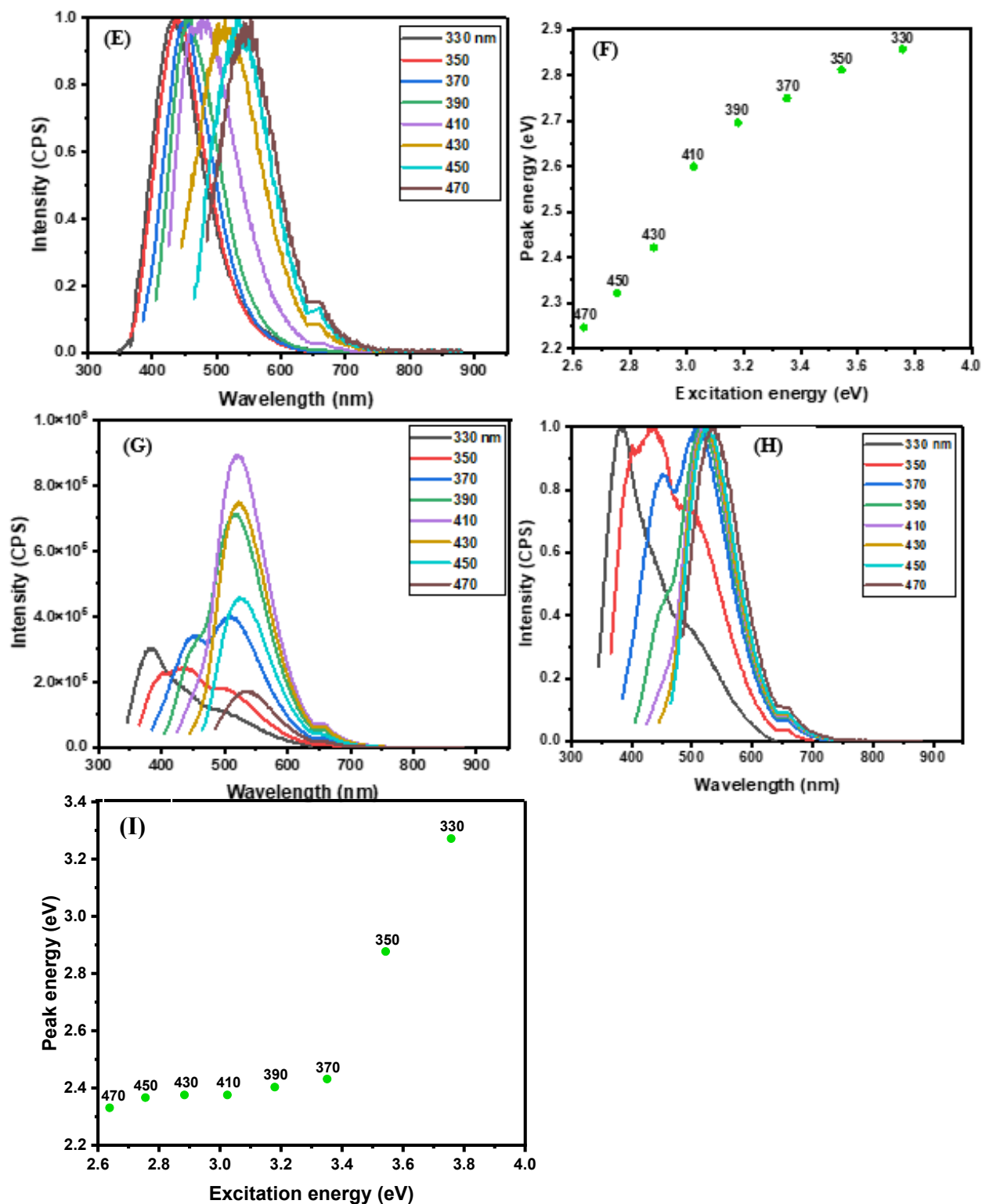


Figure 6 – A) PL spectra of CNDs (1:1) – B) Normalized PL spectra of CNDs (1:1) – C) Energy diagram of CNDs (1:1) – D) PL spectra of CNDs (4:1) – E) Normalized PL spectra of CNDs (4:1) – F) Energy diagram of CNDs (4:1) – G) PL spectra of CNDs (1:4) – H) Normalized PL spectra of CNDs (1:4) – I) Energy diagram of CNDs (1:4).

Since the main idea of this study was related to modifying the amount of functional groups of CNDs, analyzing FTIR spectra was one of the most crucial characterization techniques. In the FTIR analysis of CNDs (fig. 7D) the spectra exhibited several characteristic peaks at 3406 cm^{-1} and at 3199 cm^{-1} which could be assigned to -NH_2 (ν_{NH}) and -COOH groups (ν_{OH}), respectively. There were sp^2/sp^3 -CH at the wavelength of 3072 and 2776 cm^{-1} . The breadth suggested the presence of -COOH (1697 cm^{-1}) group. They had -C=O/-C=N bonds (1600 cm^{-1}), aromatic carbon (1355 cm^{-1}) and -C=N (1184 cm^{-1}). The different ratios between the reagents were clearly visible through FTIR. Firstly, for 4:1 CNDs, there was a significant increase in the prominence of 1697 cm^{-1} band which was assigned to ν_{OH} respect to the one at 1600 cm^{-1} (typical of amine groups). This result was the first confirmation of the increasement in the amount of -COOH groups due to the high amount of citric acid. The opposite happened with the 1:4 CNDs that contained more amine groups and more aromatic groups due to the abundance of urea. Then, another important finding was caught at C=N at 1184 cm^{-1} where the peak was more pronounced for CNDs (4:1), compared to the other ones. That wavelength indicated the bond within the plans N-doped, the presence of these N heteroatoms belonged to the higher amount of citric acid compared to that of urea.

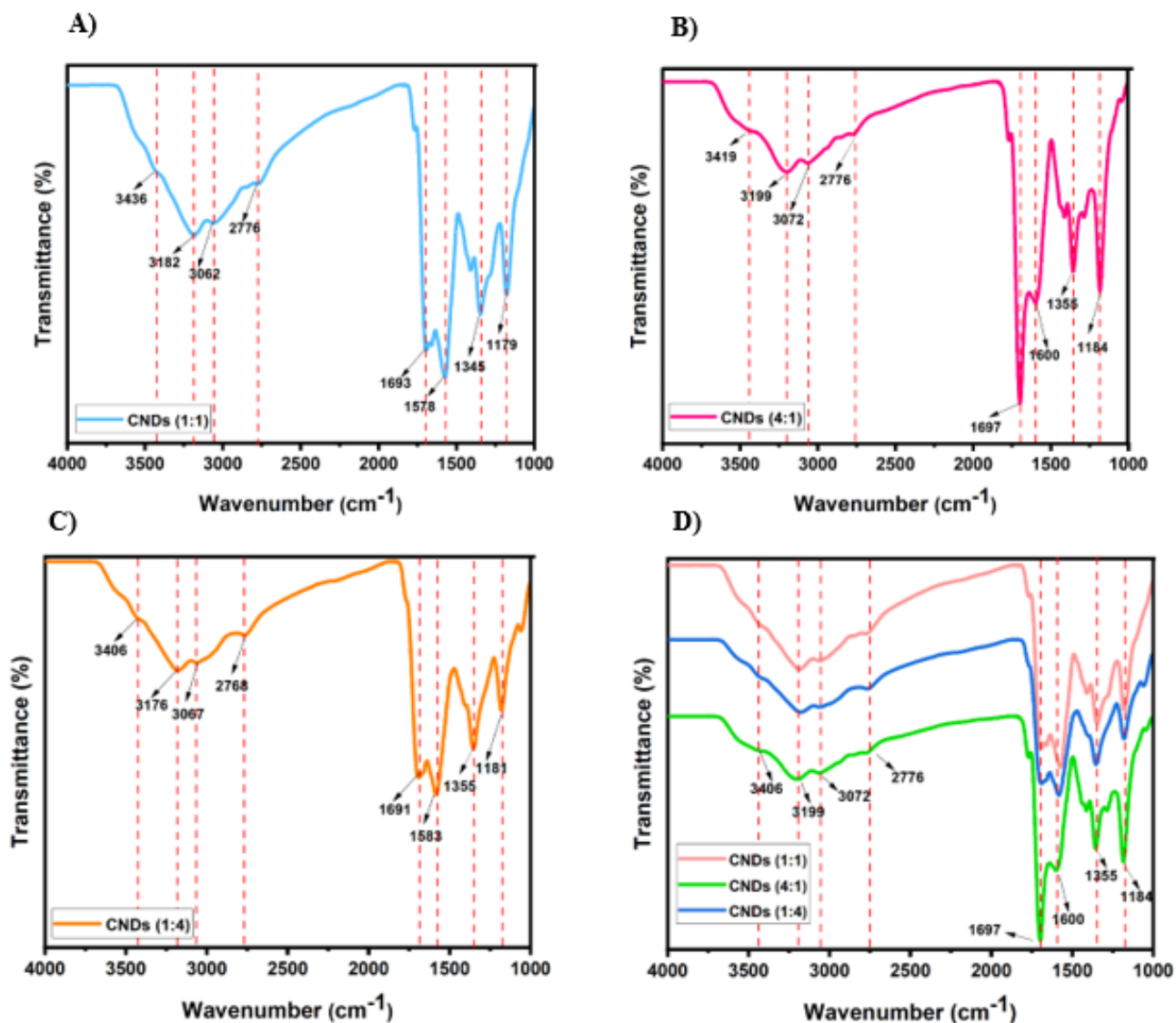


Figure 7 – A) FTIR of CNDs (1:1) – B) FTIR of CNDs (4:1) – C) FTIR of CNDs (1:4) – D) FTIR spectrum comparison between the CNDs.

The UV/vis spectroscopy of P-CDs (fig. 8 - A, B, C, D) showed two distinguishable peaks: the absorption band at 241 nm, assigned to π - π^* electronic transition of C=C and the broad band at 351 nm, attributed to n- π^* electronic transition of the C=O and/or the C=N structures. Clearly, by comparing all the four kinds of P-CDs, in the fig. 8 E, the P-CDs with less citric acid and more PEHA or the same quantity respect to the other ones presented the two peaks deeper. Each P-CDs had a concentration of 0.02 mg/ml.

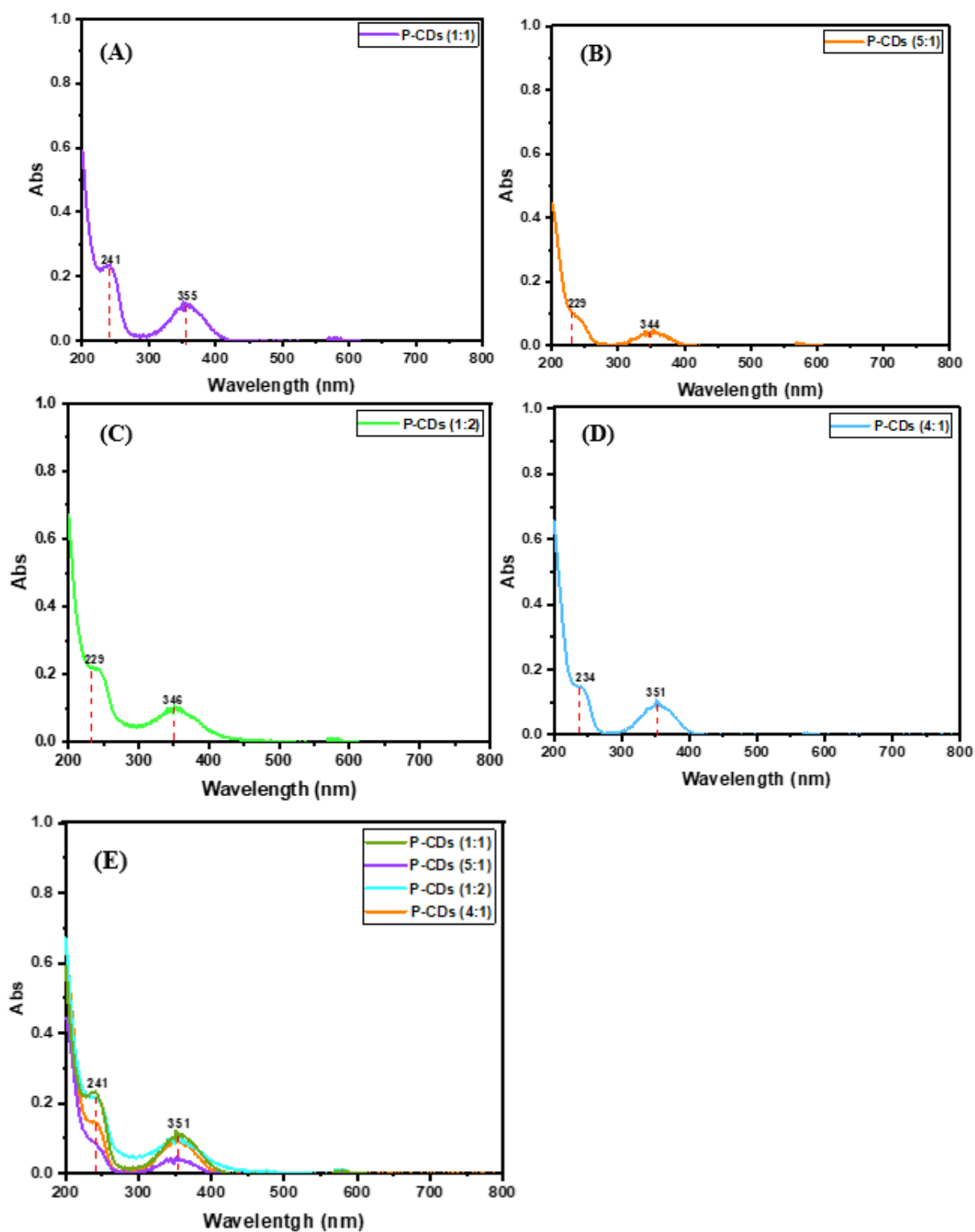


Figure 8 – **A)** UV/vis of P-CDs (1:1) – **B)** UV/vis of P-CDs (5:1) – **C)** UV/vis of P-CDs (1:2) – **D)** UV/vis of P-CDs (4:1) – **E)** UV/vis spectrum comparison between the P-CDs.

The fluorescence emission spectra of P-CDs (fig. 9 - A, B, C, D) showed an excitation-independent-emission in the range of 400-600 nm with the maximum PL emission at 438 nm (the one of (5:1) P-CDs was at 451 nm) upon the excitation of 370

nm for all the P-CDs unless (1:2) P-CDs that had the maximum PL emission upon the excitation at the wavelength of 350 nm. The wavelength range used was between 330 nm (3.78 eV) and 470 (2.67 eV) nm. By analyzing the PL emission spectra, there were not relevant differences between the P-CDs. The P-CDs (1:1) and P-CDs (1:2) had a concentration of 0.25 $\mu\text{g/ml}$, P-CDs (5:1) of 0.125 $\mu\text{g/ml}$ and P-CDs (4:1) of 0.0625 $\mu\text{g/ml}$.

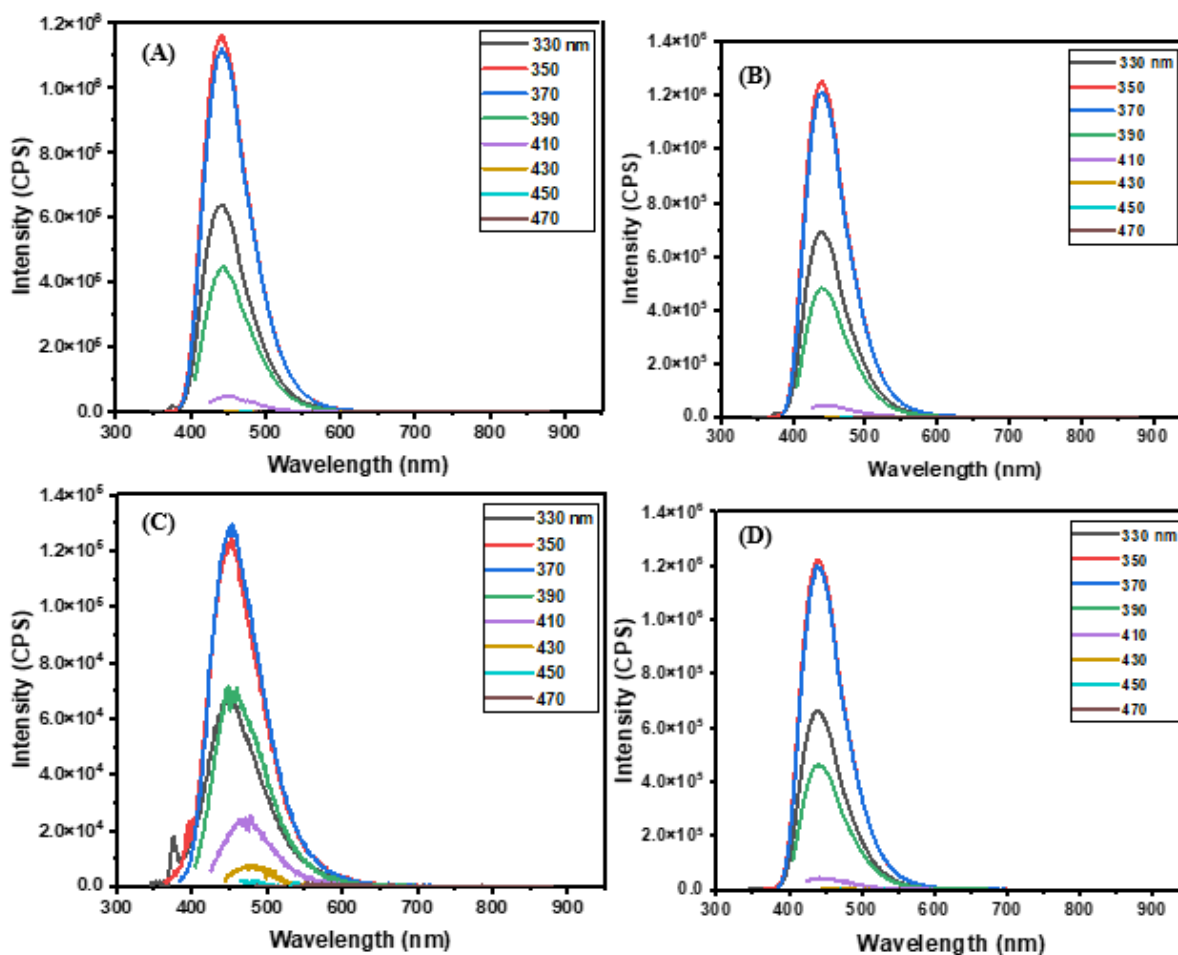
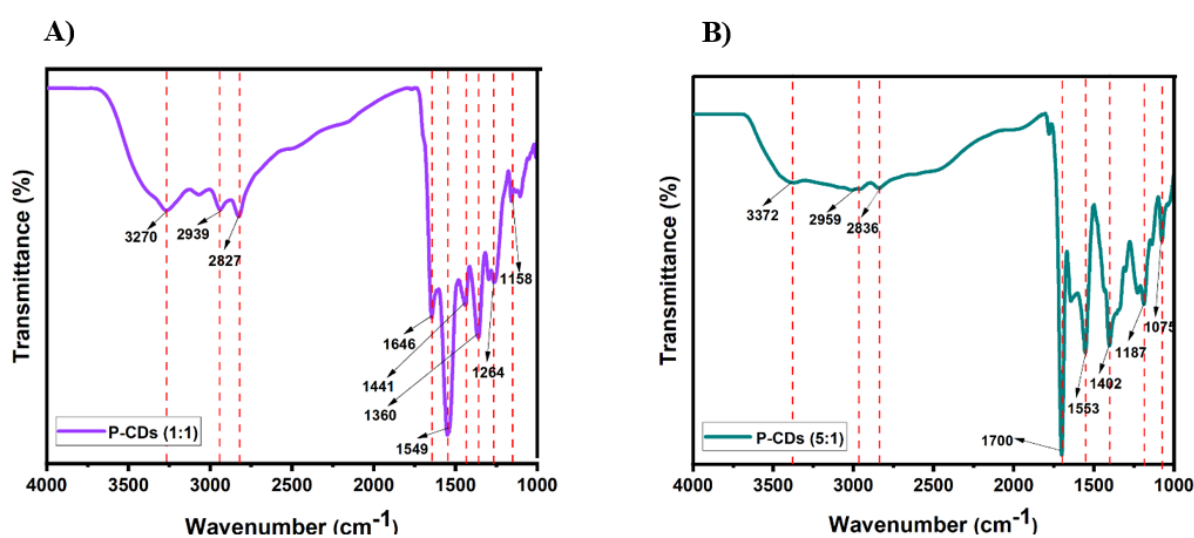


Figure 9 – A) PL spectra of P-CDs (1:1) – B) PL spectra of P-CDs (5:1) – C) PL spectra of P-CDs (1:2) – D) PL spectra of P-CDs (4:1).

Fig. 10 - A, B, C, D showed the FTIR spectrum of P-CDs (1:1), (5,1), (1:2) and (4,1), respectively. In order to identify the functional groups of P-CDs, the FTIR spectrum of P-CDs (fig. 10E) showed a broad band at 3278 cm^{-1} , indicating δ_{NH} or δ_{OH} . Bands at 2940 and 2834 could be assigned to the ν_{CH} and 1444 cm^{-1} corresponding to the δ_{CH} . The other

peaks at 1699, 1643, 1552, 1363, 1299 and 1114 cm^{-1} denoted $\nu_{\text{C-O}}$, $\nu_{\text{C-O}}$, δ_{NH} , $\nu_{\text{C-O}}$, $\nu_{\text{C-N}}$ and δ_{OH} , respectively. However, some differences between the P-CDs were evident. For instance, the peak at 1643 cm^{-1} ($\nu_{\text{C-O}}$) that indicated the presence of carboxylic and carbonylic groups (aldehydes and ketones) was less pronounced than the one at 1552 cm^{-1} , typical of amine groups in (1:1) and (1:2) P-CDs because these kinds of CDs contained more $-\text{NH}_2$ groups due to the abundant quantity of PEHA, an organic amine. On the other hand, from the FTIR spectrum, the confirmation that (5:1) and (4:1) P-CDs had more citric acid than the other two was given by confronting the peak at 1699 cm^{-1} with the one at 1552 cm^{-1} : the first one was deeper due to carboxylic groups.



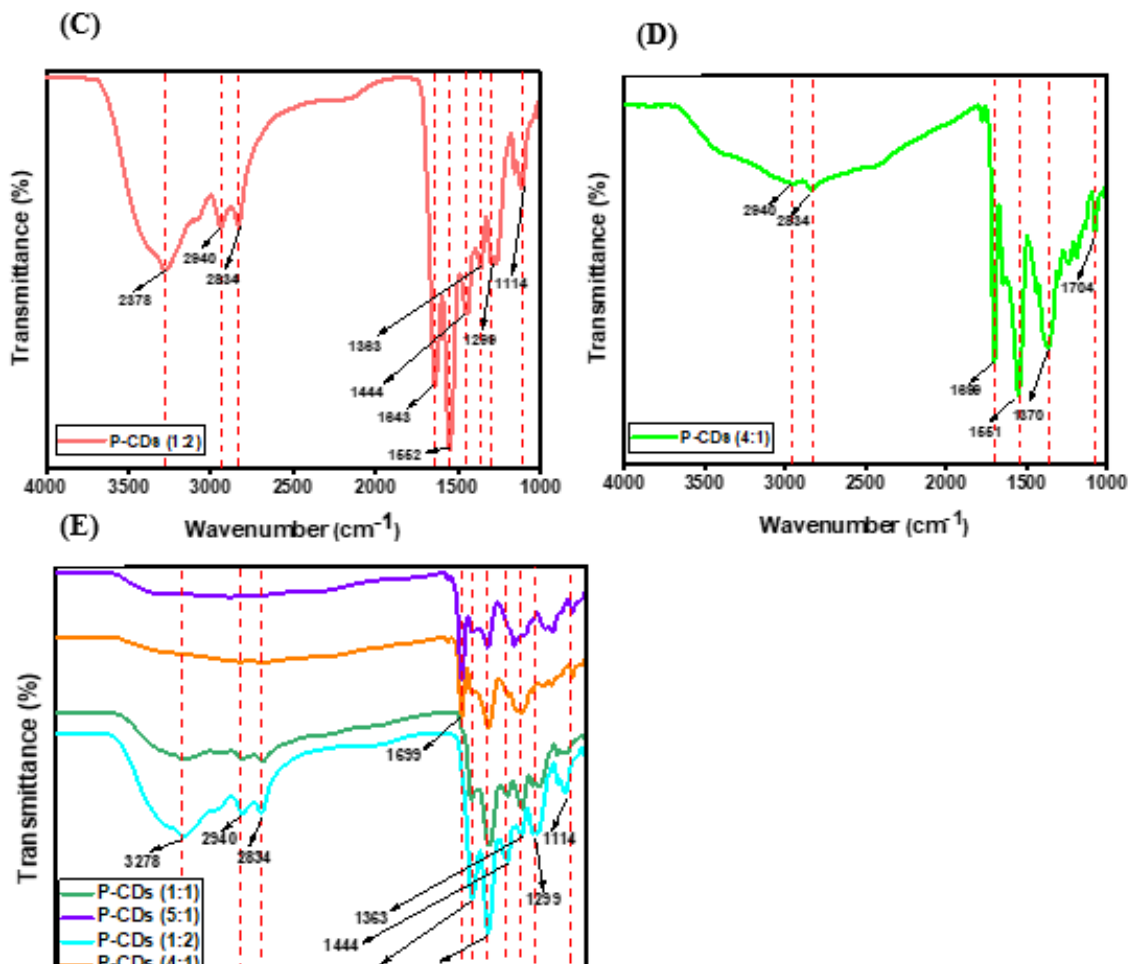


Figure 10 – **A**) FTIR of P-CDs (1:1) – **B**) FTIR of P-CDs (5:1) – **C**) FTIR of P-CDs (1:2) – **D**) FTIR of P-CDs (4:1) – **E**) FTIR spectrum comparison between the P-CDs.

As evident by the UV/vis absorption spectrum of G-CDs (fig. 11D), the band at 231 nm showed aromatic C=C π - π^* and the band at 332 nm was due to the presence of C=O/C=N bonds with n- π^* transition. At reaction temperatures below the melting point (153 °C), citric acid molecules were constrained in the crystal lattice. As the reaction temperature was increased, more citric acid actively participate in the reaction with EDA to extend the conjugation [23]. The concentration was 3.9 mg/ml.

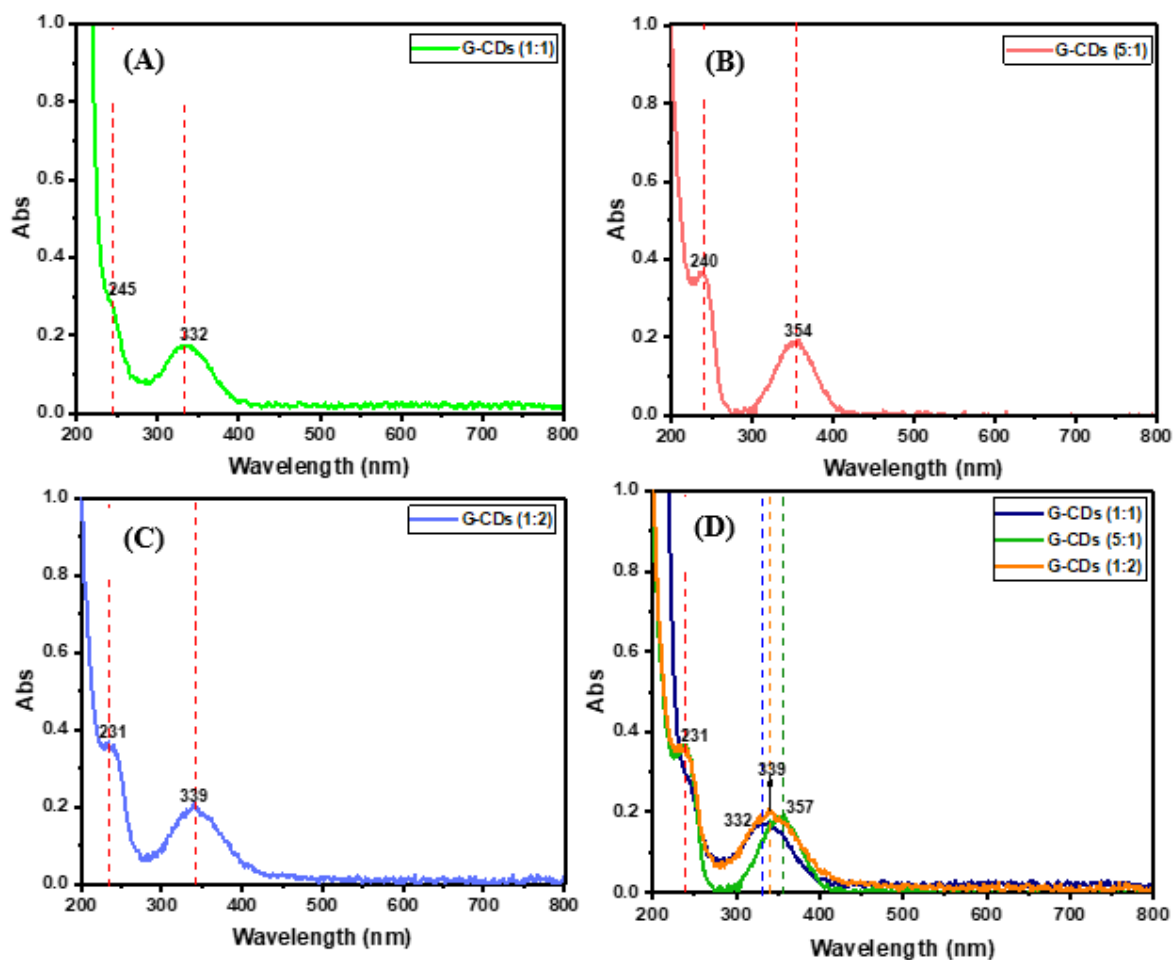


Figure 11 – A) UV/vis of G-CDs (1:1) – B) UV/vis of G-CDs (5:1) – C) UV/vis of P-CDs (1:2) – D) UV/vis spectrum comparison between the P-CDs.

Based on the fluorescence emission spectra (fig. 12A), as well as corresponding normalized spectra (fig. 12B), G-CDs were excited at wavelengths ranging from 330 nm (3.78 eV) to 470 nm (2.67 eV) and G-CDs (1:1) showed the maximum emission wavelength of 450 nm upon excitation of 350 nm. G-CDs presented excitation-dependent-emission in the low energy region ($\lambda > 400$ nm), whereas an excitation-wavelength-independent PL in the high energy region ($\lambda < 400$ nm). This last behavior could be result from the relatively pure surface of the G-CDs caused by complete passivation of EDA. Instead, the wavelength-dependent PL behavior could be exhibited by the G-CDs that are covered by less EDA, which would leave many surface defects on the G-CDs to generate many energy levels in the energy gap between the HOMO (highest occupied molecular orbital) and LUMO (lowest unoccupied molecular orbital), and this would cause many emissive traps [23]. Instead, regarding G-CDs (5:1) and G-CDs (1:2), they presented excitation-independent-emission with the maximum intensity at 450 nm upon the excitation of 350 nm and 370 nm, respectively (fig 12 – D, E). The

energy plots of 1:1 G-CDs (fig. 12C) showed a single peak at the excitation wavelength of 330 nm. The concentration was 0.0033 mg/ml.

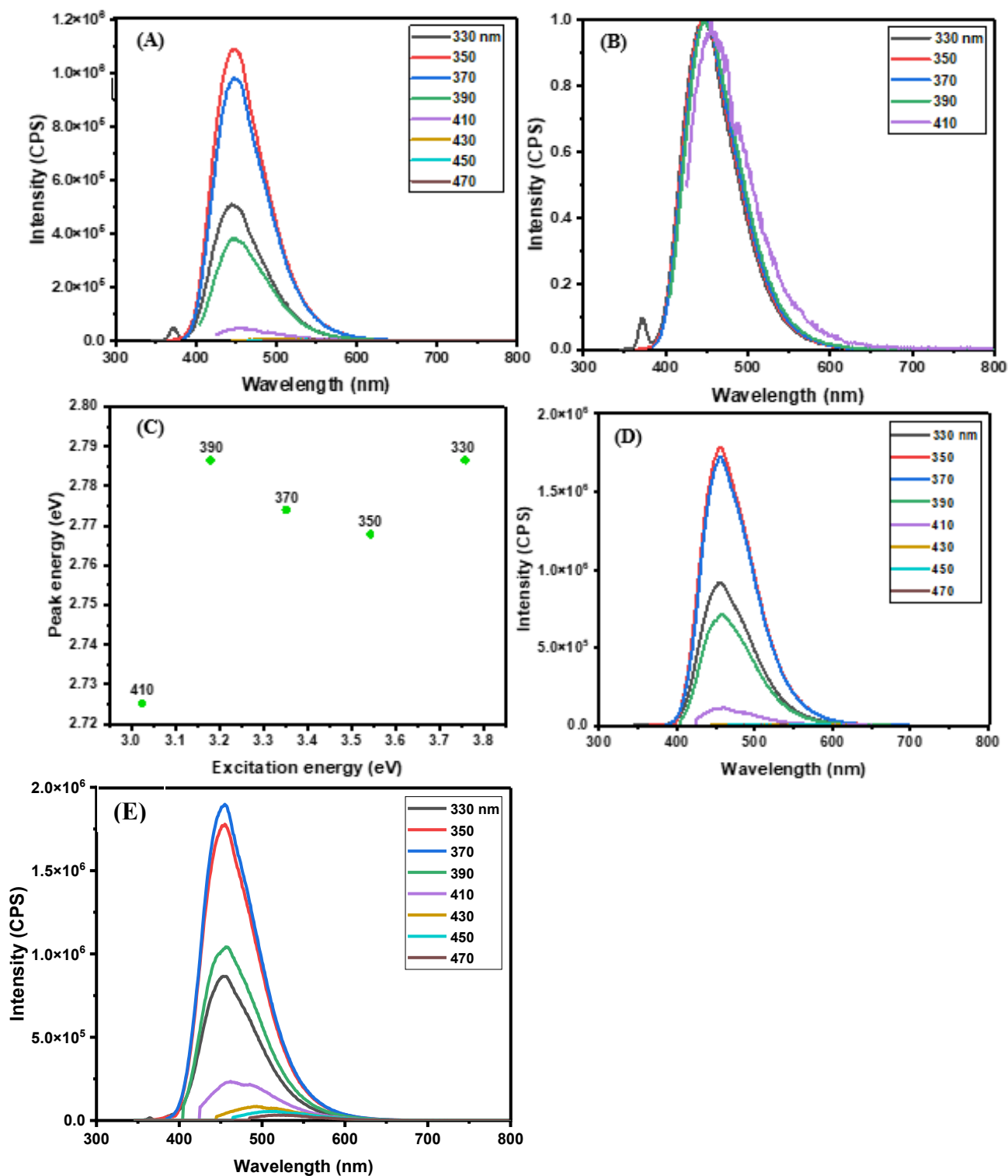


Figure 12 – A) PL spectra of G-CDs (1:1) – B) Normalized PL spectra of G-CDs (1:1) – C) Energy diagram of G-CDs (1:1) – D) PL spectra of G-CDs (5:1) – E) PL spectra of G-CDs (1:2).

FTIR spectrum of G-CDs (fig. 13D) revealed ν_{NH} and/or ν_{OH} (3268-3071 cm^{-1}), ν_{CH} (2935-2874 cm^{-1}), $\nu_{\text{C-O}}/\nu_{\text{C-N}}/\nu_{\text{C-C}}$ (1643 cm^{-1}), δ_{NH} (1539 cm^{-1}), ρ_{CH} (1431-1368 cm^{-1}) and $\nu_{\text{C-O}}$ (1106 cm^{-1}). Among them the presence of $-\text{NH}_2$ and $-\text{OH}$ ensured a good water dispersity of G-CDs. The different ratios between the reagents were clearly visible through FTIR. Firstly, for 1:2 CNDs, there was a significant increase in the prominence of 3268 cm^{-1} band which was assigned to ν_{NH} respect to the one at 3268 cm^{-1} (typical of amine groups). This result was the first confirmation of the increasement in the amount of $-\text{NH}_2$ groups due to the high amount of EDA. The opposite happened with the 1:1 CNDs that contained less EDA, in which the peaks at 2935-2874 cm^{-1} were deeper than the one at 3268 cm^{-1} for the presence of carboxylic groups.

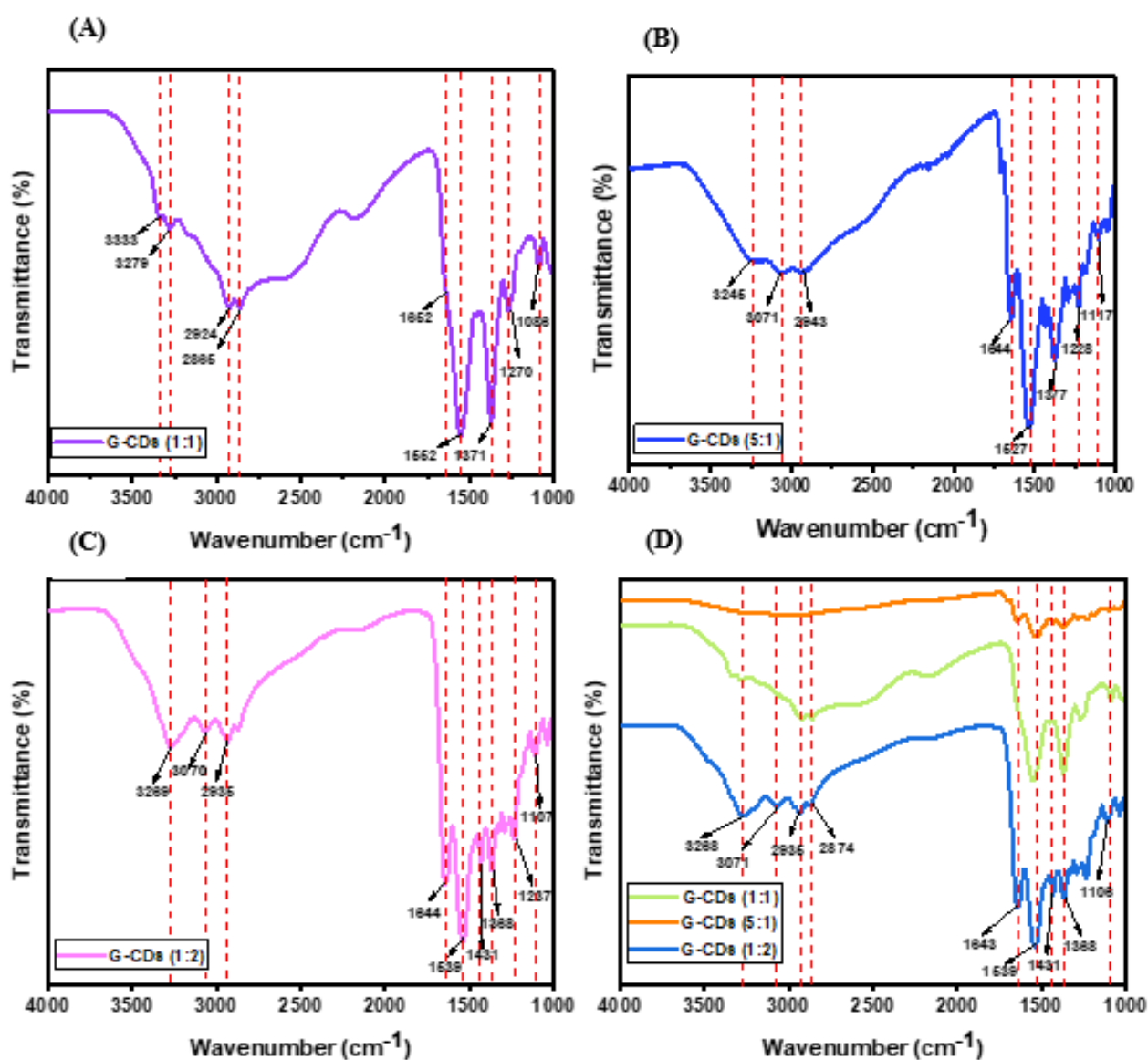


Figure 13 – A) FTIR of G-CDs (1:1) – B) FTIR of G-CDs (5:1) – C) FTIR of G-CDs (1:2) – D) FTIR spectrum comparison between G-CDs.

UV/vis spectra of Y-CDs (fig. 14) revealed two peaks: 232 nm assigned to C=C and 289 nm attributed to C=O with n- π^* electron transition. The concentration of the solution was 0.01 mg/ml.

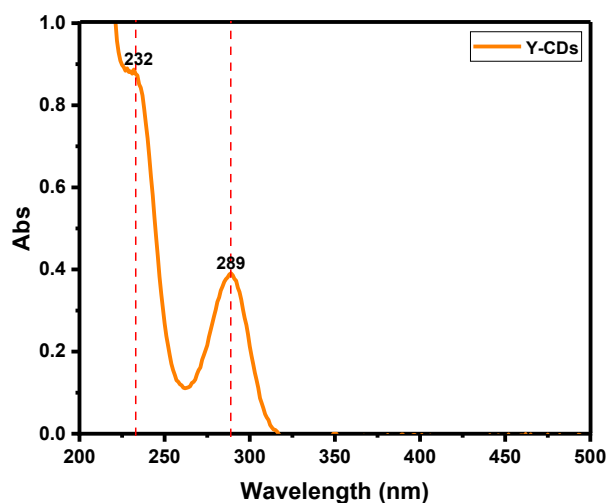


Figure 14 – UV/vis spectra of Y-CDs.

By analyzing the PL spectrum of Y-CDs (fig. 15), as the emission wavelength changed from 330 to 470 nm, the PL intensity increased at first and the decreased after reaching a maximum excitation value with $\lambda = 410$ nm. Hence, the PL behavior was excitation-independent-emission with the maximum PL emission at 573 nm, so without blue/red shift with the change of excitation wavelengths. These results were usually attributed to surface state emission. The concentration was 0.01 mg/ml.

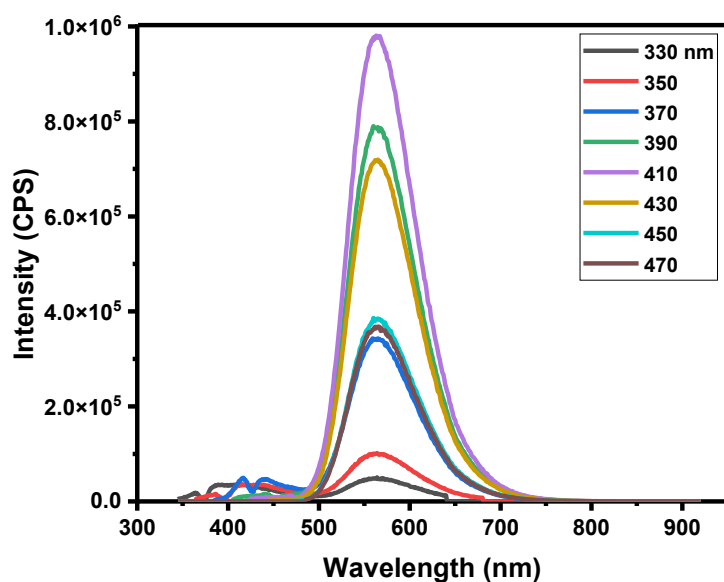


Figure 15 – PL spectra of Y-CDs.

FTIR spectrum of Y-CDs (fig. 16) revealed ν_{OH} at 3385 cm^{-1} , ν_{NH} at 3193 cm^{-1} , $\nu_{\text{C-N}}$ at 1630 cm^{-1} , δ_{NH} at 1590 cm^{-1} , $\nu_{\text{C-N}}$ at 1499 cm^{-1} , $\nu_{\text{C-O}}$ at 1272 and $\nu_{\text{C-N}}$ at 1155 cm^{-1} indicating the presence of many nitrogen-containing groups.

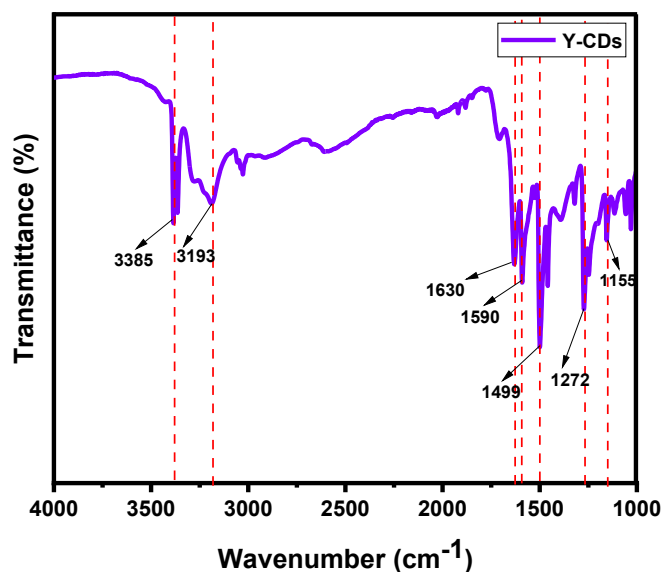


Figure 16 – FTIR spectra of Y-CDs.

3.2 CO₂ adsorption

Thermogravimetric analysis, TGA, was conducted using a Netzsch TG 209 F3 Tarsus thermo-microbalance (Netzsch, USA) under nitrogen gas and carbon dioxide. This technique measured the changing of the mass related to temperature which was used in the optic to study the CO₂ adsorption capacity of different kinds of CDs both in natural state and both dehydrated. The purpose of this study was designing the CD with the highest CO₂ uptake capacity and compare it with other chemical structure and materials already analyzed in literature in order to prepare biocompatible filters for CO₂ for the implantology field or facial breathing devices.

3.2.1 TGA without the dehydration step

In detail, in order to investigate the CO₂ adsorption capacity of CDs in natural state, TGA was conducted in absence of the dehydration step. During the TGA process (fig. 17) the mass of the specimen had to be at least 5 mg and it was placed inside a crucible made of Al₂O₃ with a mass of 239.5 mg. There were 3 important steps to follow. Initially, the

temperature was kept steady at 25 °C for 2 h with injection of pure CO₂ (99.9 %) with a pressure of 15 psi (103 kPa) at a flow rate of 10 ml/min to adsorb CO₂ reversibly. Subsequently, the gas flow was changed from CO₂ to pure N₂ (99.995%) with a pressure of 15 psi (103 kPa) at a flow rate of 10 ml/min while the temperature increased from 25 to 100 °C at a rate of 10 °C/min to desorb CO₂. After the temperature reaches 100 °C, it started to decrease to 25 °C with a rate of 2 °C/min. The change in the weight of specimen during adsorption/desorption processes, measured through TGA, was used to calculate the CO₂ adsorption capacity of CDs. N₂ was flushed during the desorption process because it is an inert gas so it will not have any interactions with CDs. Instead, the normal atmosphere contains O₂ that can oxidize the amines on CDs while changing their CO₂ adsorption capacity. The fig. 18 showed the setup for CO₂/N₂ selectivity tests by TGA.



Figure 17 – TGA process for CDs in natural state.

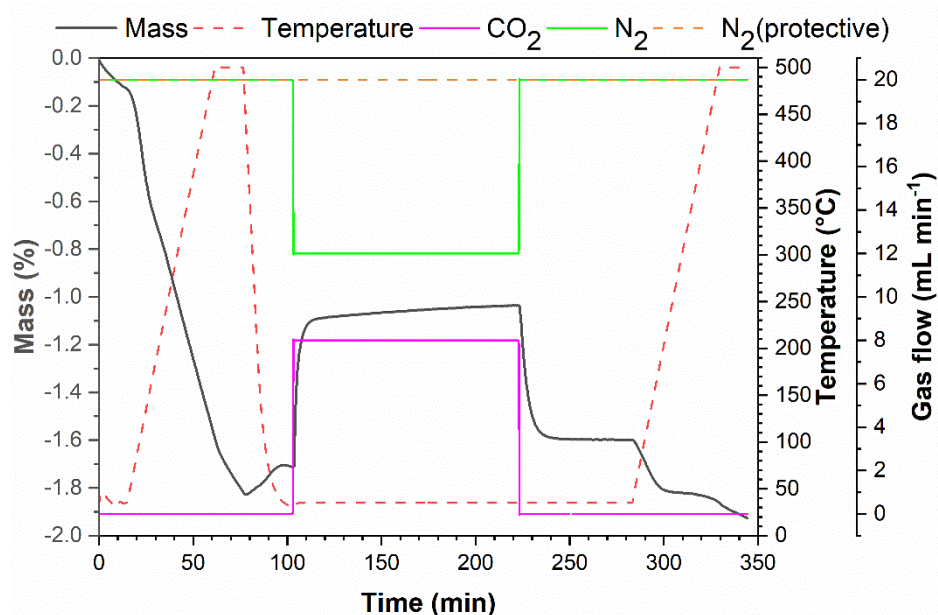


Figure 18 – Setup for CO₂/N₂ selectivity tests by TGA.

Fig. 19, 20, 21, 22 showed the CO₂ uptake results of different CDs. The CO₂ adsorption capacity was calculated as the following formula: Q (capacity: mg/g) = ((weight after CO₂ adsorption) – (weight before CO₂ adsorption)) / (weight before CO₂ adsorption). In the

capacity unit: mg/g, mg indicated the amount of CO₂ that had been adsorbed and g indicated the quantity of adsorbent (CDs) that had been used during the process. The CO₂ adsorption capacities were obtained from the TGA curves with three replicates and summarized in **Table 1**. According to **Table 1**, the CO₂ adsorption capacities of different CDs species can be arranged in the order of CNDs, Y-CDs < P-CDs < G-CDs. Regarding CNDs, the second replica displayed a CO₂ adsorption of 0 % that was considered an outlier value. Among different CDs species, G-CDs exhibited a high CO₂ adsorption capacity of 67 mg/g. It might be associated with the highest amine content in G-CDs. This hypothesis was further supported by a high CO₂ adsorption capacity (140.0 mg/g) of PEHA, an amine-abundant precursor of P-CDs, and its TGA curves are shown as fig. 23. Furthermore, for PEHA, considering the higher mass increase during CO₂ adsorption process than the mass decrease in the CO₂ desorption process, it was likely that CO₂ molecules were bound by the amine groups of PEHA to form stable amide bonds.

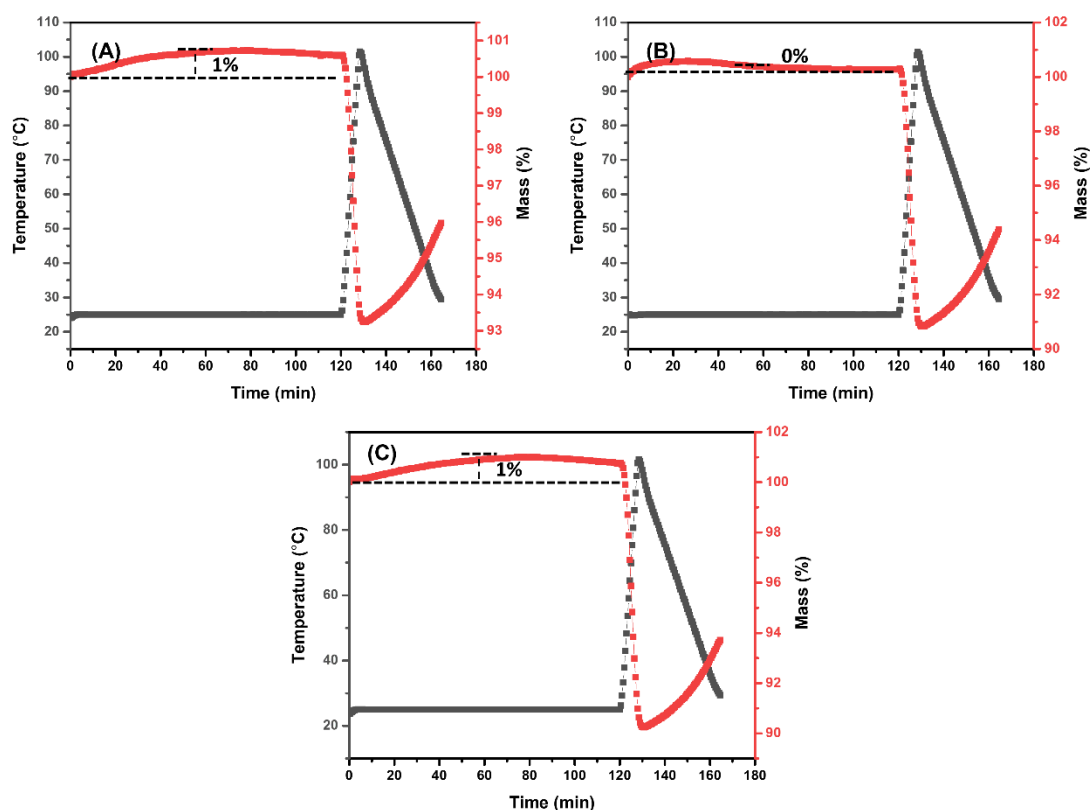


Figure 19 – TGA of CNDs in natural state in CO₂ adsorption and desorption processes over time. Three replicates are exhibited as (A-C).

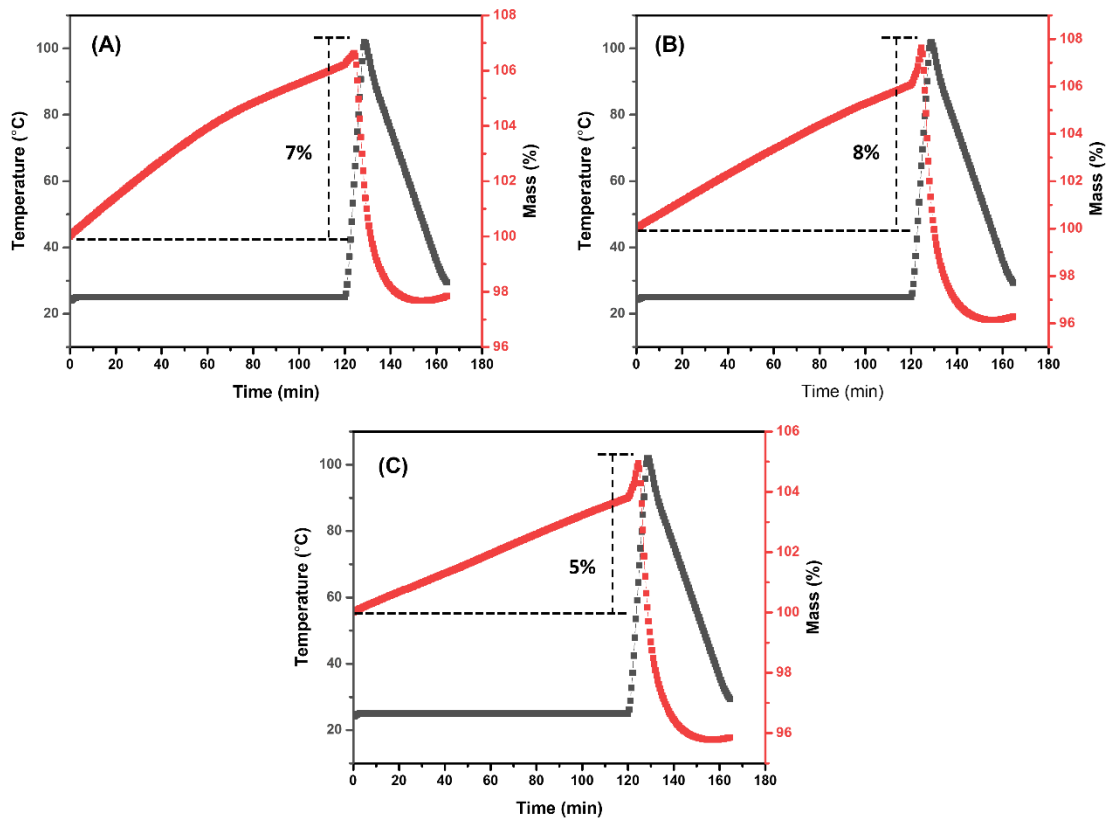


Figure 20 – TGA of G-CDs in natural state in CO₂ adsorption and desorption processes over time. Three replicates are exhibited as (A-C).

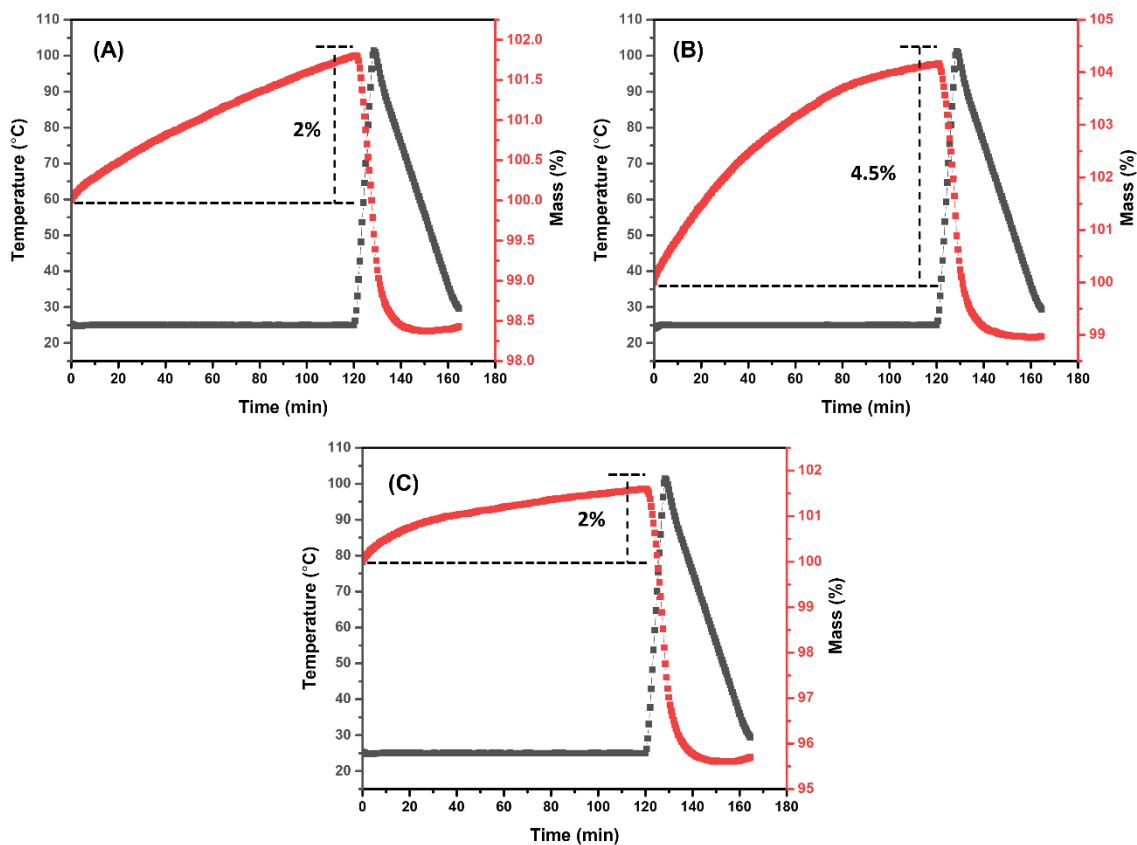


Figure 21 – TGA of P-CDs in natural state in CO₂ adsorption and desorption processes over time. 41 Three replicates are exhibited as (A-C).

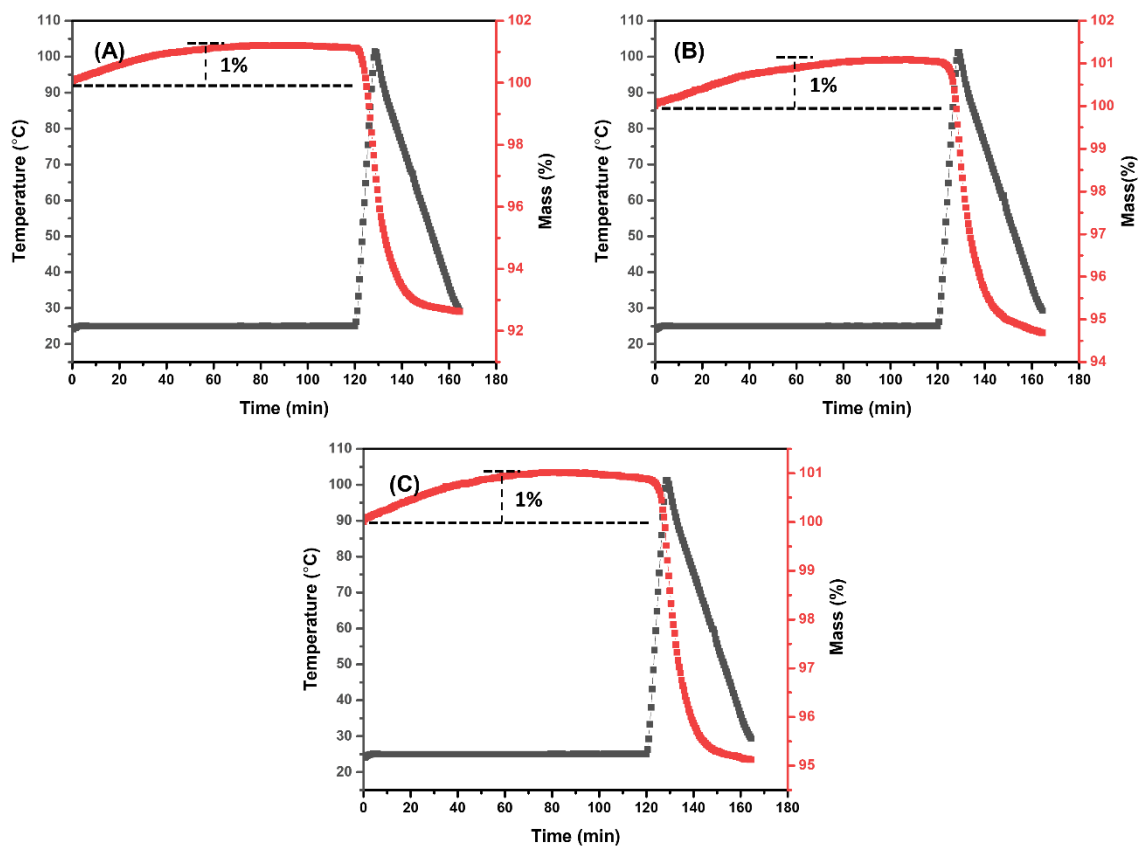


Figure 22 – TGA of Y-CDs in natural state in CO₂ adsorption and desorption processes over time. Three replicates are exhibited as (A-C).

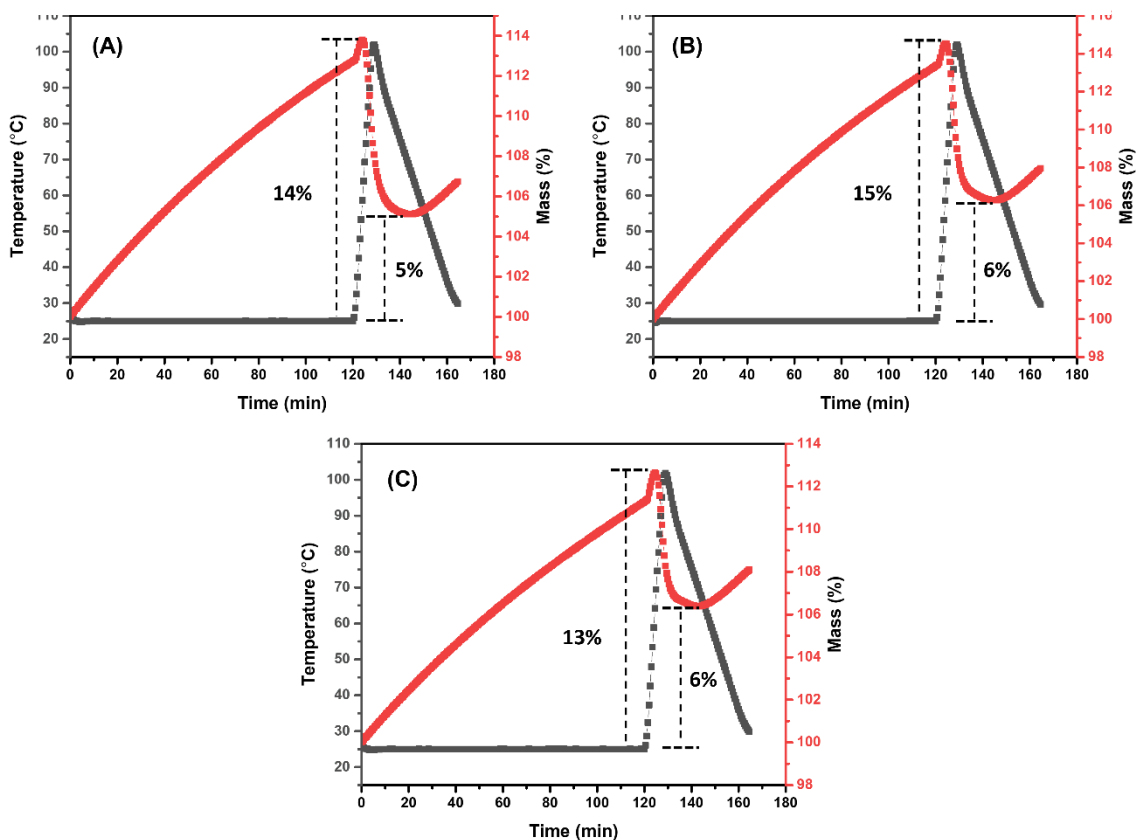


Figure 23 – TGA of PEHA in natural state in CO₂ adsorption and desorption processes over time. Three replicates are exhibited as (A-C).

CD species	Replicate 1 (mg/g)	Replicate 2 (mg/g)	Replicate 3 (mg/g)	Average (mg/g)
CNDs	10.0	0	10.0	10.0 ± 0.1
G-CDs	70.0	80.0	50.0	67.0 ± 15.0
P-CDs	20.0	45.0	20.0	28.0 ± 13.0
Y-CDs	10.0	10.0	10.0	10.0 ± 0.1

Table 1 – CO₂ adsorption capacities of CDs.

3.2.2 TGA with the dehydration step

After identifying the best performing CDs, in terms of CO₂ adsorption capacity, TGA was conducted with the presence of the dehydration process as the first step while the second step included all the process of the previous TGA. For this reason, the whole experiment was longer than the previous one, it took in total 4 h and 10 min instead of 2 h and 45 min. The choice to introduce the dehydration step was related to the reducing of the CO₂ adsorption capacity due to the presence of water molecules. This was caused by the competition between CO₂ and H₂O for the same adsorption sites. Due to its dipole moment, H₂O strongly interacted with the adsorption sites of CDs.

The TGA process was repeated 18 times, 3 times for each sample, including P-CDs with the two modified ones and G-CDs with the two modified ones. Regarding the dehydration step, the mass of the sample had to be at least 5 mg and it was placed inside a crucible made of Al₂O₃ with a mass of 239.5 mg. Initially, the temperature increased to 100 °C with a rate of 10 °C/min for 7 min and 30 s. Subsequently, with injection of pure N₂ (99.99 %) with a pressure of 15 psi (103 kPa) at a flow rate of 10 ml/min, the temperature was kept steady at 100 °C for 40 min to remove moisture from CDs, after this time it started to decrease to 25 °C with a rate of 2 °C/min. Then, the following step was identical to the entire CDs TGA process in their natural state. The whole process was showed in fig. 24.

The TGA graphs of G-CDs (1:1), (1:2), (5:1) and P-CDs (1:1), (1:2), (5:1) are showed in fig. 25, 27, 28, 26, 29 and 30, respectively.



Figure 24 – Schematic TGA process of CDs with an initial dehydration step.

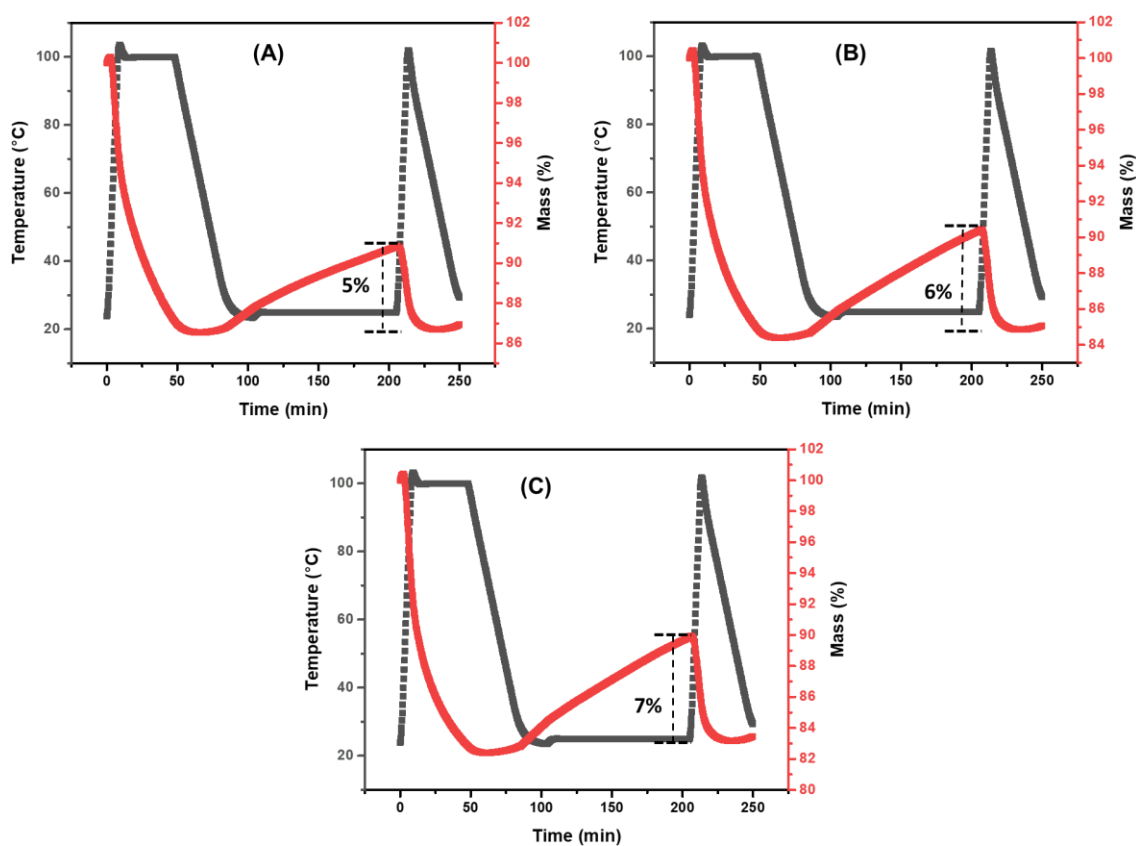


Figure 25 – TGA of G-CDs (1:1) in the absence of moisture in CO₂ adsorption and desorption processes over time. Three replicates are exhibited as (A-C).

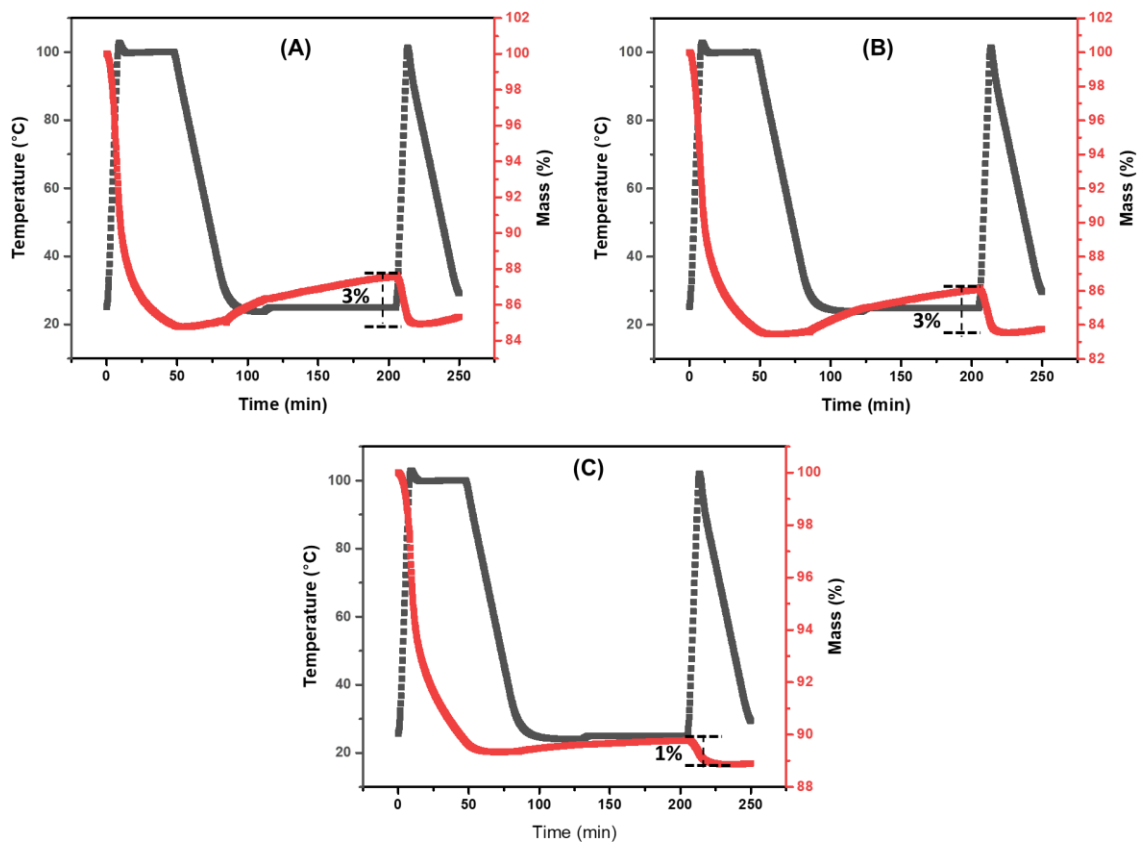


Figure 26 – TGA of P-CDs (1:1) in the absence of moisture in CO₂ adsorption and desorption processes over time. Three replicates are exhibited as (A-C).

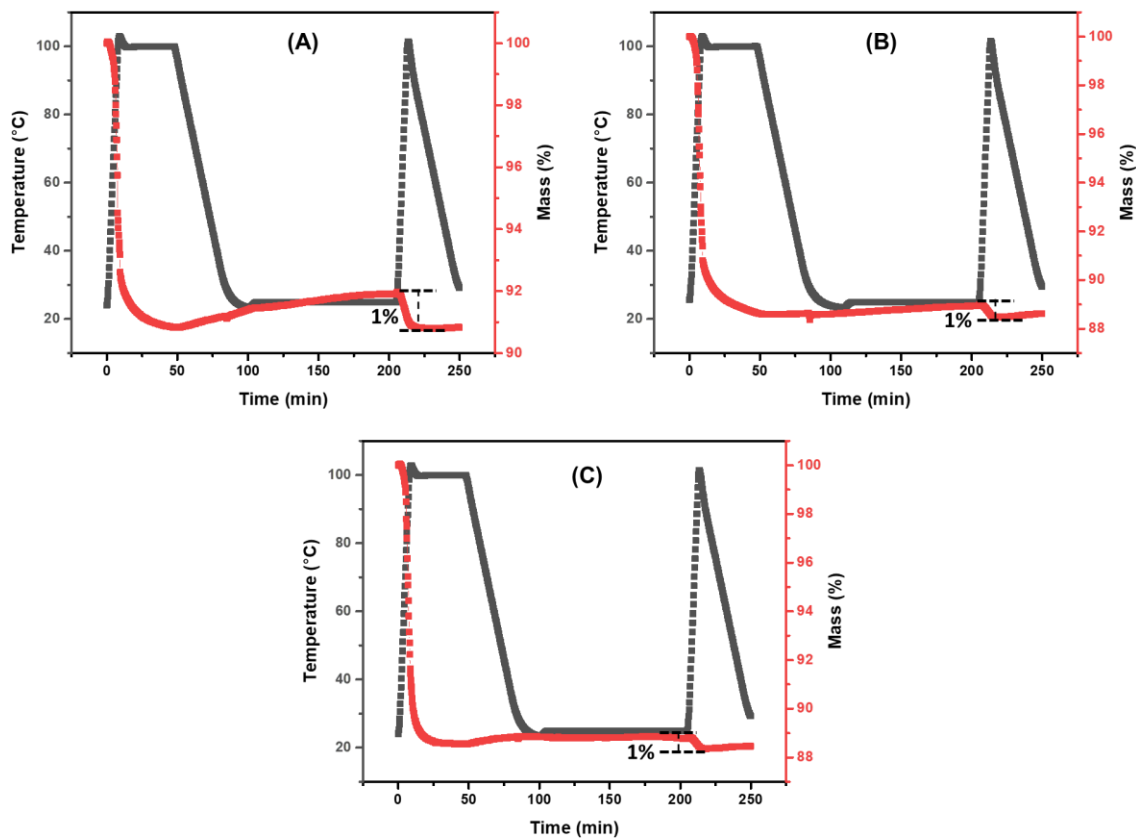


Figure 27 – TGA of G-CDs (1:2) in the absence of moisture in CO₂ adsorption and desorption processes over time. Three replicates are exhibited as (A-C).

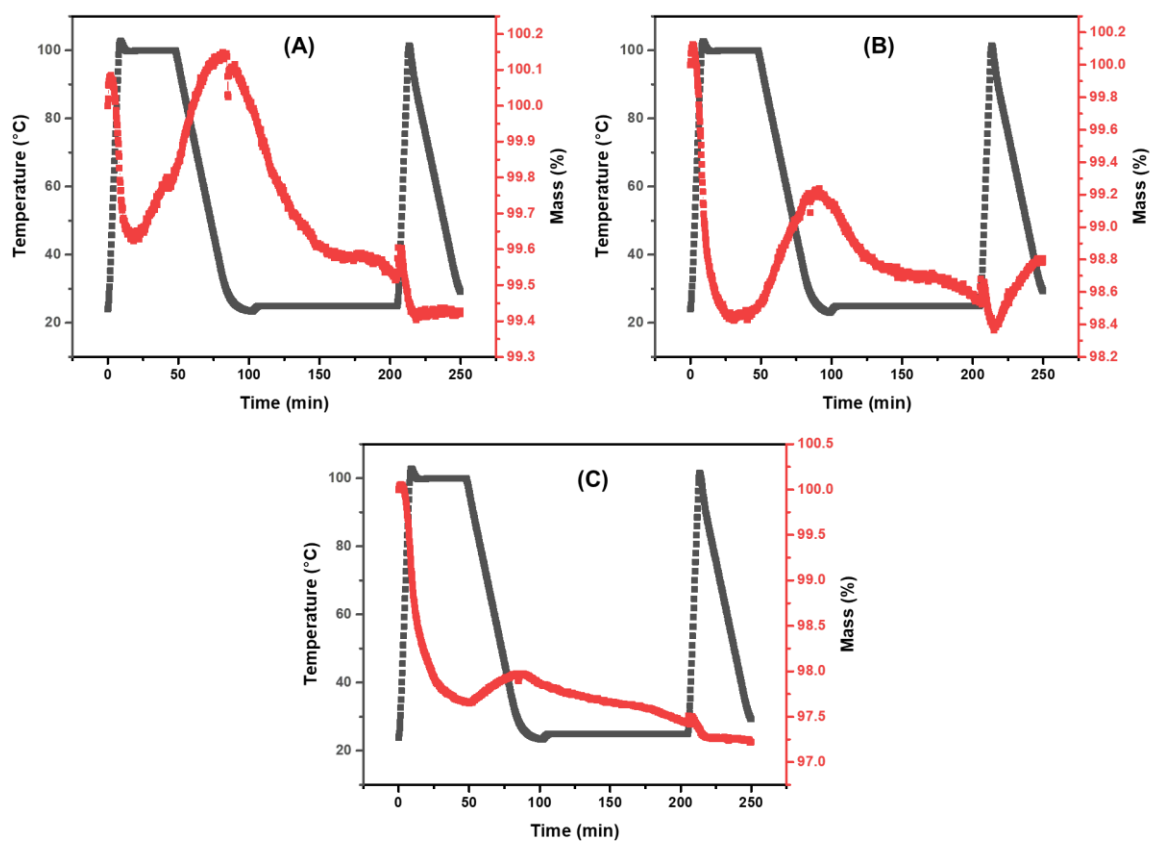


Figure 28 – TGA of G-CDs (5:1) in the absence of moisture in CO₂ adsorption and desorption processes over time. Three replicates are exhibited as (A-C).

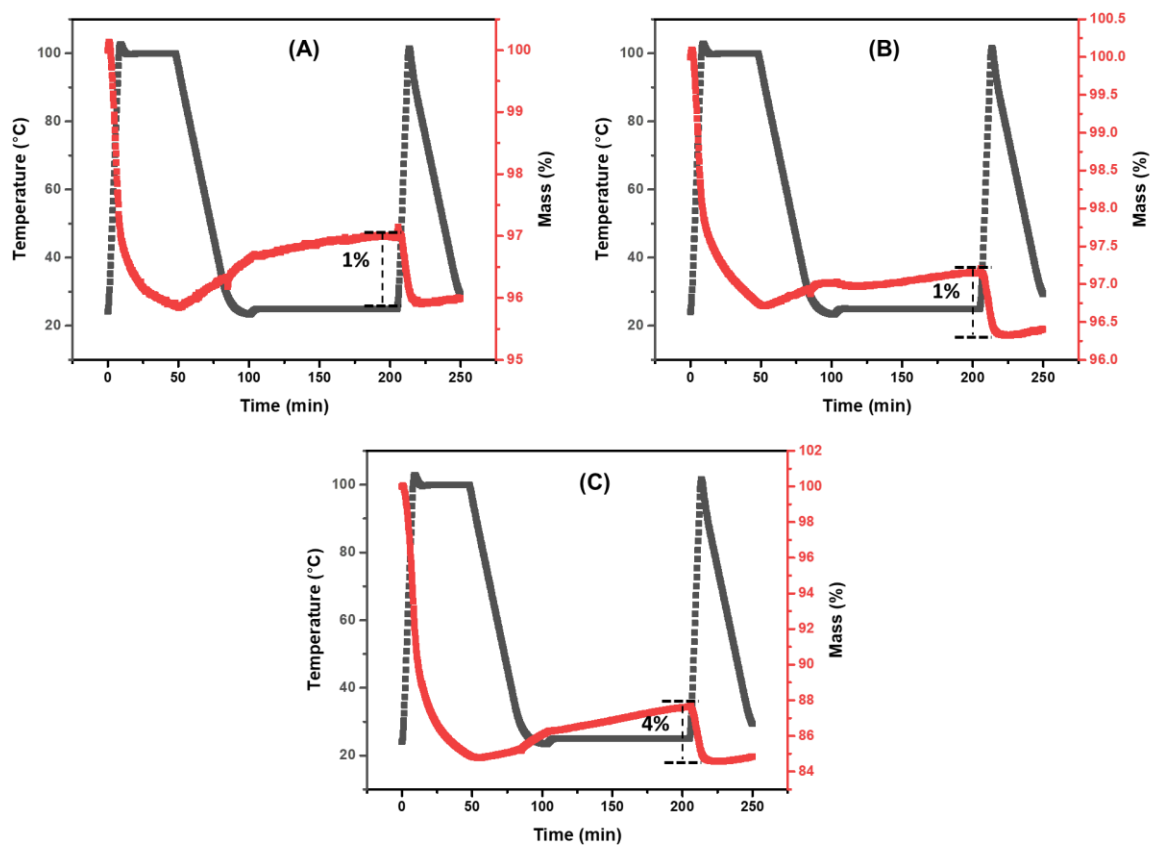


Figure 29 – TGA of P-CDs (1:2) in the absence of moisture in CO₂ adsorption and desorption processes over time. Three replicates are exhibited as (A-C).

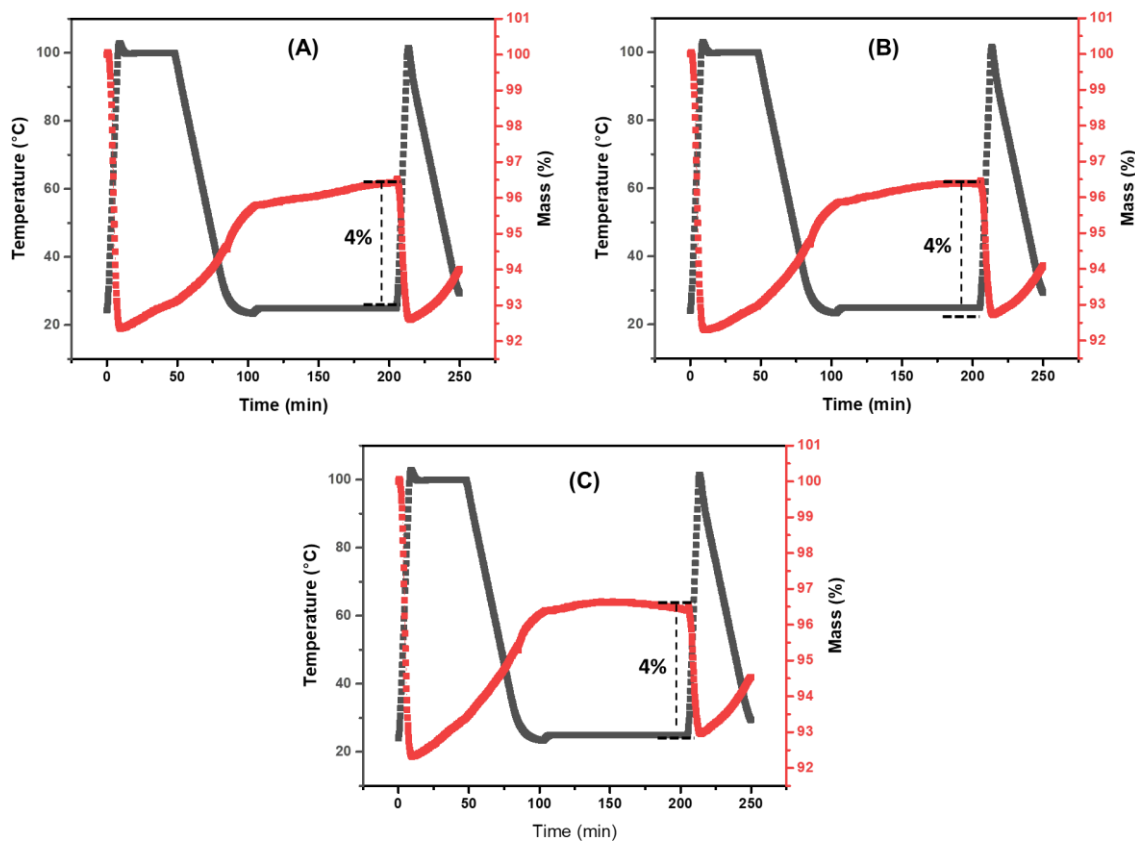


Figure 30 – TGA of P-CDs (5:1) in the absence of moisture in CO₂ adsorption and desorption processes over time. Three replicates are exhibited as (A-C).

CO₂ can be adsorbed by water to form carbonic acid. In order to exclude the impacts of moisture on the CO₂ uptake measurements, TGA was performed on G-CDs and P-CDs that showed higher CO₂ uptake capacities with a new method to remove the adsorbed water on both CDs before the ventilation of CO₂ flux. After the removal of moisture from the surface of CDs, TGA revealed that the CO₂ uptake capacities of G-CDs and P-CDs were 60 mg/g and 23 mg/g, respectively (**Table 2**). Compared to the natural states, dry G-CDs and P-CDs showed slight reductions in the CO₂ uptake capacities, which demonstrated a non-negligible impact of adsorbed water on the CO₂ uptake of CDs.

Furthermore, to elucidate the functionalities especially between -OH and -NH₂ that determines the CO₂ uptake capacities of CDs, G-CDs and P-CDs were modified by changing the molar ratios among reaction precursors. To avoid confusion, the original G-CDs and P-CDs were renamed as G-CDs (1:1) and P-CDs (1:1), respectively. Meanwhile, the G-CDs and P-CDs derived from fewer acids were named G-CDs (1:2) and P-CDs (1:2), respectively. On the contrary, synthesized with fewer amines, the G-CDs and P-CDs were named G-CDs (5:1) and P-CDs (5:1), respectively. According to **Table 2** that

summarized the CO₂ adsorption capacities of different CDs with three replicates, it was observed that with the decrease of acids in the reaction precursors, the CO₂ uptake capacity of G-CDs was significantly reduced. However, with the decrease of amines, TGA showed a complicated CO₂ adsorption and desorption process although the CO₂ adsorption capacity was also greatly lowered, which leads to a conclusion that both -OH and -NH₂ impact the CO₂ uptake of G-CDs together with a hypothesis that G-CDs after surface modification might be able to trap N₂. Compared to G-CDs, P-CDs were relatively easy to analyze, and they showed an insignificant reduction but a huge increase in the CO₂ uptake capacity with the increase and decrease of amines, respectively, in the reaction precursors, which demonstrates a dominant role of -OH in the CO₂ uptake of P-CDs. According to the TGA study, it was observed that the CO₂ uptake capacity of CDs varies among different CD species but is closely associated with the content of -OH and/or -NH₂.

CD species	Replicate 1 (mg/g)	Replicate 2 (mg/g)	Replicate 3 (mg/g)	Average (mg/g)
G-CDs (1:1)	50	60	70	60 ± 10
G-CDs (1:2)	10	10	10	10.0 ± 0.1
G-CDs (5:1)	N/A	N/A	N/A	N/A
P-CDs (1:1)	30	30	10	23 ± 10
P-CDs (1:2)	10	10	40	20 ± 15
P-CDs (5:1)	40	40	40	40.0 ± 0.1

Table 2 – CO₂ adsorption capacities of G-CDs and P-CDs under different conditions with the dehydration step.

The average of the three replicates obtained for CDs had been converted from mg/g to mmol/g to be able to compare them with other data presented in literature. So, the converted results of dehydrated-CDs were: G-CDs (1:1) up to 1.4 mmol CO₂/g, G-CDs (1:2) with 0.23 mmol CO₂/g, P-CDs (1:1) up to 0.53 mmol CO₂/g, P-CDs (1:2) with 0.45 mmol CO₂/g and P-CDs (5:1) with 0.91 mmol CO₂/g. Instead, the converted results of CDs in natural states were: 0.23 mmol CO₂/g for CNDs, 1.52 mmol CO₂/g for G-CDs, 0.64 mmol CO₂/g for P-CDs and 0.23 mmol CO₂/g for Y-CDs.

3.3 Comparison with the state of art

CO₂ is considered one of the largest drivers of global warming. In order to mitigate the emissions to the atmosphere, many possible adsorbent materials were tested in these last years, such as zeolites, amines, carbon-based, including graphene, ionic liquids...

Some studies on the CO₂ absorbed by different materials were reported and summarized below to be compared with the results especially the CO₂ absorption capacities obtained from the carbon dots used in this study.

To compare the CO₂ uptake capacities of 1°, 2° and 3° amines, (3-aminopropyl) trimethoxysilane, [3-(methylamino) propyl trimethoxysilane, and [3-(diethylamino) propyl-trimethoxysilane, were applied as the respective models. They were immobilized on highly ordered mesoporous silicas (SBA-15) and the maximum CO₂ adsorption capacities of SBA-15-NH₂ (1°), SBA-15-NH-CH₃ (2°) and SBA-15-NH(CH₂CH₃)₂ (3°), conducted at 25 °C under atmospheric condition, turned out to be were 0.95, 0.75 and 0.17 mmol CO₂/g adsorbent, respectively [24].

A good performance in terms of CO₂ adsorption was exhibited by an aerogel modified with the generation 3.0 poly(amidoamine) (PAMAM) dendrimer at a high concentration the and optimum carbon nanotubes (CNT) content, reaching a value of 2.23 mmol/g. This result is the highest reported value for dendrimer-modified graphene-oxide aerogels thus far, and it was attributed to the addition of CNTs in the hybrid aerogels [25].

Graphene, as a CO₂ adsorbent, has received wide attention because of its unique molecular structure and many properties such as tunable porosity, excellent thermal conductivity, mechanical strength, chemical stability and large accessible surface area. Moreover, the possibility of functionalizing the surface has led to the production of innovative graphene-based materials for efficiently capturing CO₂ from the atmosphere. Rao and co-workers measured CO₂ adsorption capacities of 7.80 and 8.60 mmol/g, for the graphene obtained from exfoliation of graphite oxide (GO), and thermal conversion of nanodiamonds, respectively [26]. Mishra and Ramaprabhu achieved a maximum adsorption capacity of 12 mmol/g at 11 bar 100 °C [27]. In another study, Meng and Park produced graphene nanoplatelets (GNPs) by thermally exfoliating GO sheets in vacuum and recorded an adsorption of 56.4 mmol/g at 25°C and 30 bar [28]. In addition, Ning et al. demonstrated that graphene nanomesh with inplane pores (GNMs), prepared through

chemical vapor deposition using porous layered MgO as a template, showed a CO₂ uptake capacity of 36.5 mmol/g at 1 °C and 31 bar [29]. In another study, Xia et al. synthesized graphene with trimodal micro-meso-macroporous system and reported an uptake capacity of 1.8 mmol/g of CO₂ at 0 °C and 1 bar [30]. Kim et al. fabricated a series of N- or S-doped graphene-based carbon derived from different graphene/polymer composites such as: graphene/polypyrrole, rGO/polyaniline, rGO/polyindole and rGO/polythiophene [31]. All these composites demonstrated a CO₂ uptake capacity > 4 mmol/g under ambient conditions, comparable to or even higher than many other solid adsorbents including MOFs, amine functionalized silica and activated carbon. In another research, graphene was doped with borane-tetrahydrofuran and displayed an adsorption capacity of 1.80 mmol/g. Zhou et al. studied the CO₂ adsorption of graphene with N-rich terpyridine between the sheets and the capacity was measured to be 2.70 mmol/g at 0 °C and 1 bar [32]. Similarly, Mishra and Ramaprabhu synthesized graphene/polyaniline composites and obtained an adsorption of 75 mmol/g, 3.5 times higher than that of pristine graphene (21.6 mmol/g) at 11 bar and 25 °C [33]. Another nanocomposite studied was graphene/Fe₃O₄, that was capable to adsorb CO₂ with a high capacity of 60 mmol/g at 25 °C. Moreover, graphene was functionalized with polyethyleneimine (PEI) in the optics to obtain a synergistic effect given the flexible morphology of PEI and its capacity to uptake CO₂. The result highlighted an adsorption capacity of 6.40 mmol/g at 25 °C [34]. Recently, GO-based 3D hydrogels were prepared by Sui and Han and, at a dispersion temperature of 100 °C, a capacity of 2.40 mmol/g at 0°C and 1 bar was registered [35]. Particular attention was given to GO functionalized by amines such as ethylenediamine (EDA), diethylenetriamine (DETA) and triethylenetetramine (TETA). Among them, the highest CO₂ uptake capacity, 1.10 mmol/g, was recorded for EDA [36]. Other GO nanocomposites were also analyzed. For instance, Chowdhury et al. added TiO₂ to GO with different mass ratios (0.1, 0.2, 0.3) and at the mass ratio of 0.1, due to the large specific surface area, the nanocomposite showed the highest adsorption (1.90 mmol/g at 25 °C and 1 bar) among the three [37]. Other examples of GO-based nanocomposite included GO/Cu-BTC with an adsorption capacity of 8.20 mmol/g at 0 °C and 1 bar, higher than that of pristine Cu-BTC (6.50 mmol/g under the same conditions) [38], GO/UiO-66 with 3.40 mmol/g at 25 °C and 1 bar and GO-TETA-Ac/Cu₃(BTC)₂ (triethylenetetramine acetate known as TETA-Ac) with 5.60 mmol/g at 25 °C and 1 bar [39]. Above all, the composite presented both a good cyclic adsorption/desorption stability and a high CO₂ kinetic separation [7]. Furthermore,

3D graphene with surface-microporous structure was favored in the mass diffusion project and exposure of adsorption sites for CO₂ achieving an adsorption capacity of 2.28 mmol/g that was further increased to 3.13 mmol/g by KOH activation due to the increasing oxygen-containing functional groups [40].

TTMP, a microporous organic material obtained from polymerization of 2,6,14-trithynyltritycene and 1,3,5-tris(azidomethyl)-2,4,6-trimethylbenzene, is a thermally stable polymer with a high surface area that renders it feasibility to adsorb CO₂. The CO₂ uptake reached a capacity of 163 mg/g (3.70 mmol/g) at 0 °C, while 109 mg/g (2.45 mmol/g) at 25 °C and 1 bar [41].

Zeolites, a versatile class of material, were studied as CO₂ adsorbents with especially the group of faujasite materials in particular, widely industrially synthesized. The one with low-silica content (Si/Al < 2) is called Zeolite X while the one with high-silica content (Si/Al > 2) is called Zeolite Y. In the review of Boer et al., a wide range of zeolites were analyzed at 25 °C and 1 bar, and just few of them overpassed the adsorption of 5 mmol/g such as: Na-X-zeolite (6.30 mmol/g), Li-X-zeolite (7.00 mmol/g), Ca-X-zeolite (5.20 mmol/g), Na-Y mesoporous zeolite (5.40 mmol/g) and Ca-A-zeolite (5.10 mmol/g). Zeolite X is the most well-known zeolites for CO₂ adsorption and was used as a benchmark for comparison with other adsorbents, such as carbons and MOFs [42].

In another study, Zhao et al. synthesized a series of porous carbon materials from black liquor lignin (BLL) and the material prepared by KOH activation (C-BLL-KOH) achieved the most remarkable CO₂ capture capacity which was up to 5.20, 3.60 and 2.23 mmol/g at 0 °C, 25 °C and 50 °C, respectively, with a CO₂ partial pressure of 100 kPa [43].

Moreover, ionic liquid (Ils) also exhibited a promising potential for cost-effective CO₂ capture and utilization. In the review of Lian et al. [44] different CO₂ uptake capacities were reported by ionic liquid with other materials such as: Ils + PMMA (stands for poly(methyl methacrylate)) up to 1.20 mmol/g [45], Ils + SBA-15 up to 2.15 mmol/g [46], Ils + MCM-41 up to 1.84 mmol/g [47], Ils + mesoporous alumina up to 1.20 mmol/g [48], and Ils + titanate nanotubes (TNT) up to 2.46 mmol/g [49].

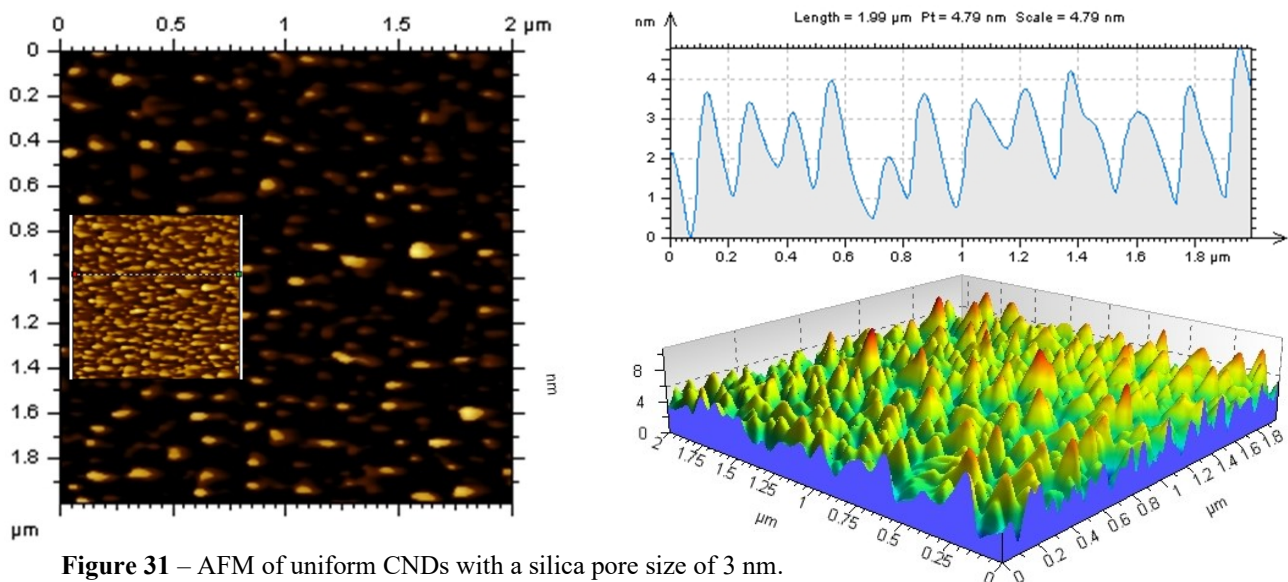
3.4 Uniform structure of CNDs

As already mentioned in the introduction, another goal of this study was to prepare uniform CNDs in order to deepen their structure characteristics related to their properties. In the optic to obtain the most uniform CNDs in size, different batches were prepared thanks to the use of silica particles, with a pore size of 3 nm or 6 nm, and the short heating time (5 min) in the autoclave that allowed to have heating homogeneity and fast heat transfer.

Each prepared sample was analyzed by AFM with a concentration of 0.1 mg/ml and, where possible, the spectrum obtained by FTIR, UV/vis and fluorescence was also recorded and studied.

In total, six batches were prepared, including one with just pure Silica, to understand if it alone could have contributed to some results in terms of homogeneity.

The first batch (fig. 31) was prepared with a SiO₂ pore size of 3 nm, as shown in the AFM analysis the distribution was peaked and the CNDs were uniform in size with an average high of 3.5 nm. Other batches had been prepared in order to find the one with the highest homogeneity.



The second batch (fig. 32) was prepared with a SiO₂ pore size of 6 nm and salts. The AFM, that showed the z-axis of CNDs, evidenced an inhomogeneity profile, higher than

the first prepared uniform CNDs because it presented a high value of variance, each peak was further than the medium value respect to the first batch AFM profile.

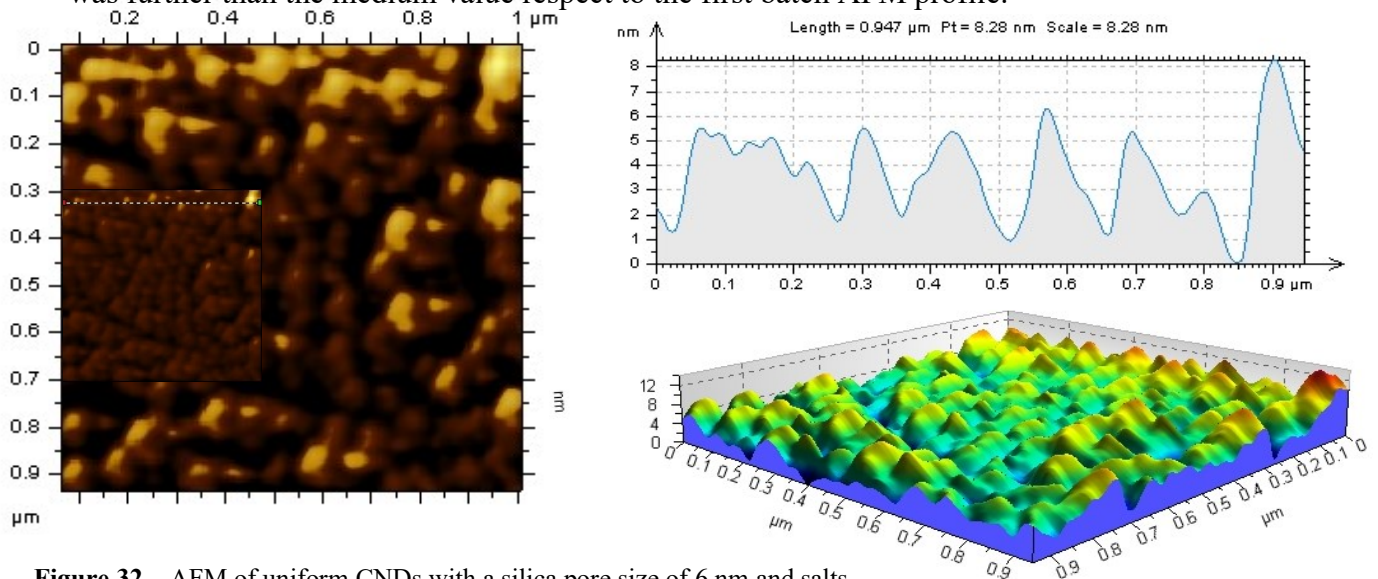


Figure 32 – AFM of uniform CNDs with a silica pore size of 6 nm and salts.

The third batch (fig. 33) was made of a SiO₂ pore size of 3 nm and salts but the inhomogeneity of the particles was high and as showed in fig. 34A the silica was not completely removed, the peak at 1074 cm⁻¹ was due to the presence of SiO₂, evidenced in fig. 34B with the FTIR spectrum of pure Silica.

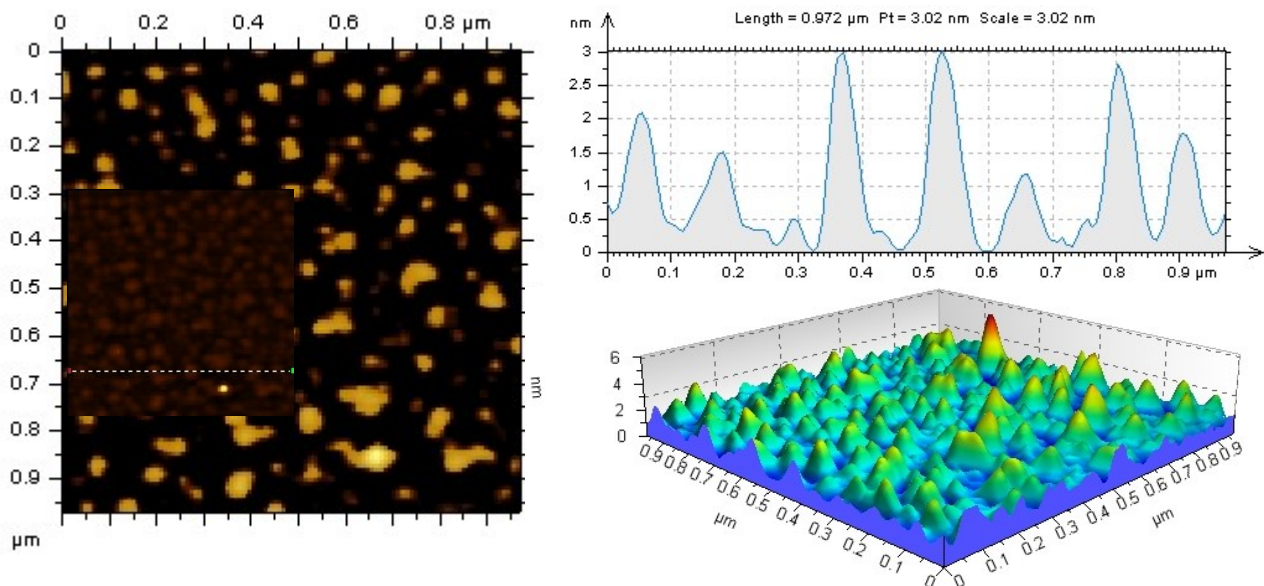


Figure 33 – AFM of uniform CNDs with a silica pore size of 3 nm and salts.

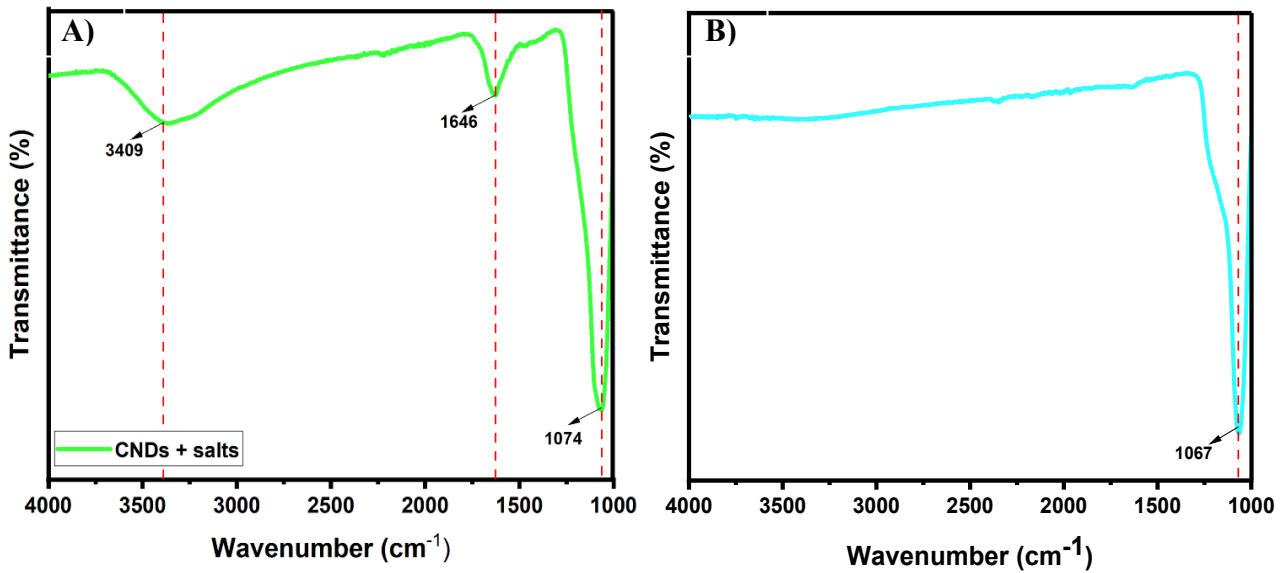


Figure 34 – A) FTIR of uniform CNDs with a silica pore size of 3 nm and salts – B) FTIR of pure SiO₂.

In the optic to remove the silica, DMF was chosen to be insoluble with silica but to be able to solubilize CNDs during the centrifugation process so as to discard the precipitant. Next, to be removed, DMF was steamed in the rotary evaporator, but it formed a sort of polymer (fig. 36), this film was present in two reactions. The AFM (fig. 35) showed high particles peaks, by meaning that CNDs were not pure so this batch had to be discarded.

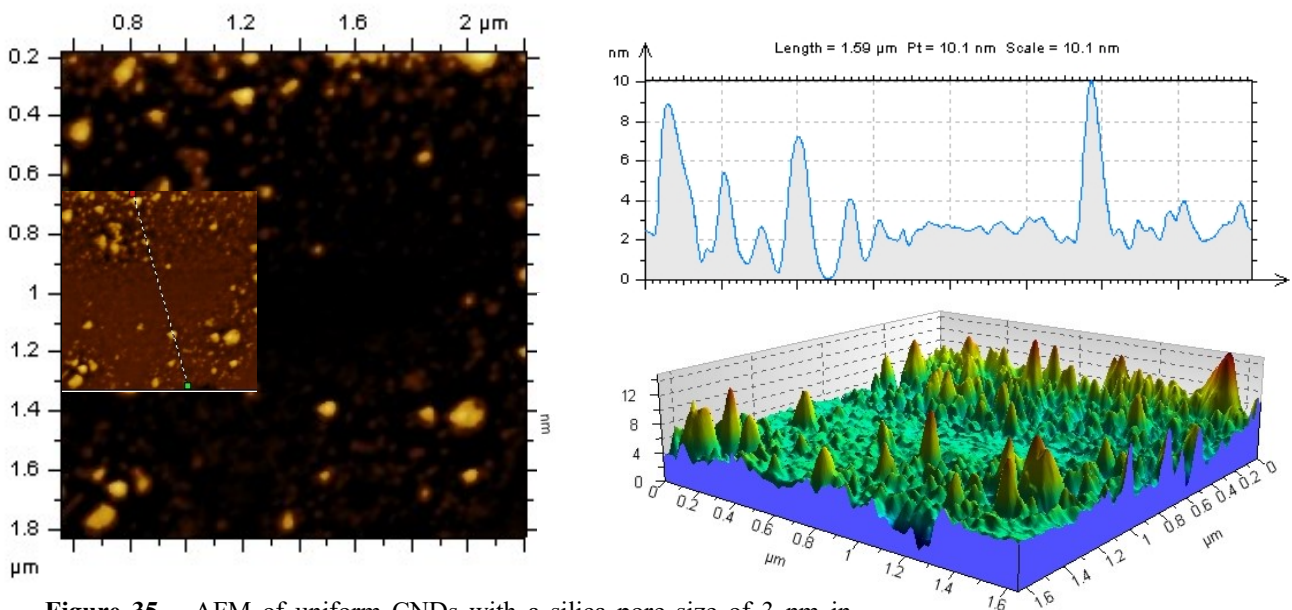


Figure 35 – AFM of uniform CNDs with a silica pore size of 3 nm in DMF.



Figure 36 – Film after the rotary evaporator in DMF.

Moreover, to be sure that the particle of silica that had been used were pure, a batch with just SiO_2 was prepared, as evidenced in fig. 37, SiO_2 alone was not able to create any uniform structures.

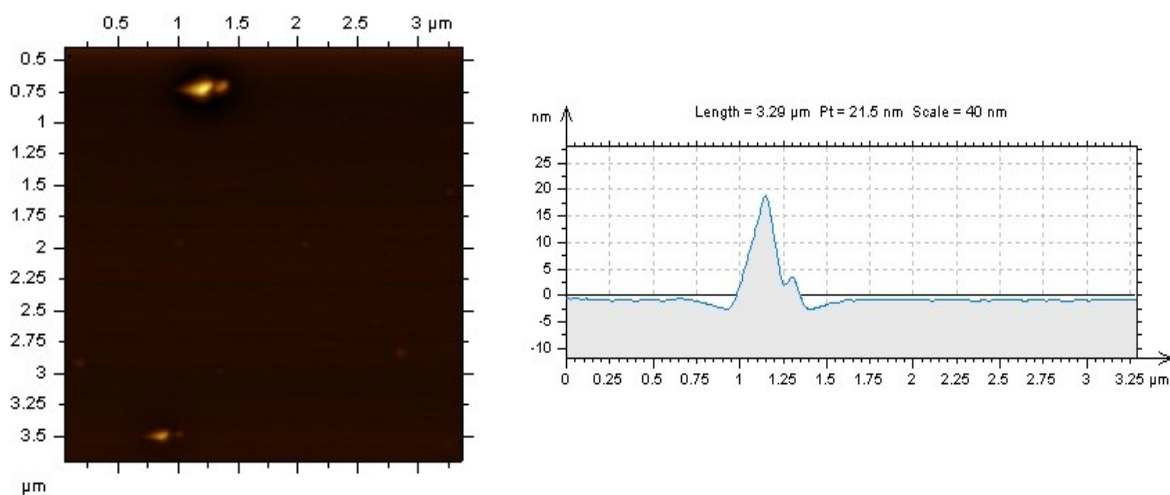


Figure 37 – AFM of SiO_2 .

Concluding, given that so far the first batch gave the best results, another identical batch was prepared and compared to the first one and to normal CNDs, without Silica, in terms of AFM (fig. 38), UV/vis (fig. 39A), FTIR (fig. 39B) and fluorescence (fig. 40). By comparing the AFM, both of them had a high grade of uniformity in the shape and size of CNDs. The UV/vis graph evidenced the same peaks for all the CNDs, the FTIR showed that uniform CNDs had the same peak correlated to the wavenumber of CNDs, by meaning that the structure was the same and that all the silica reacted with urea and citric acid. Furthermore, all the three PL spectra were similar, stating that uniform CNDs were synthesized in the correct way.

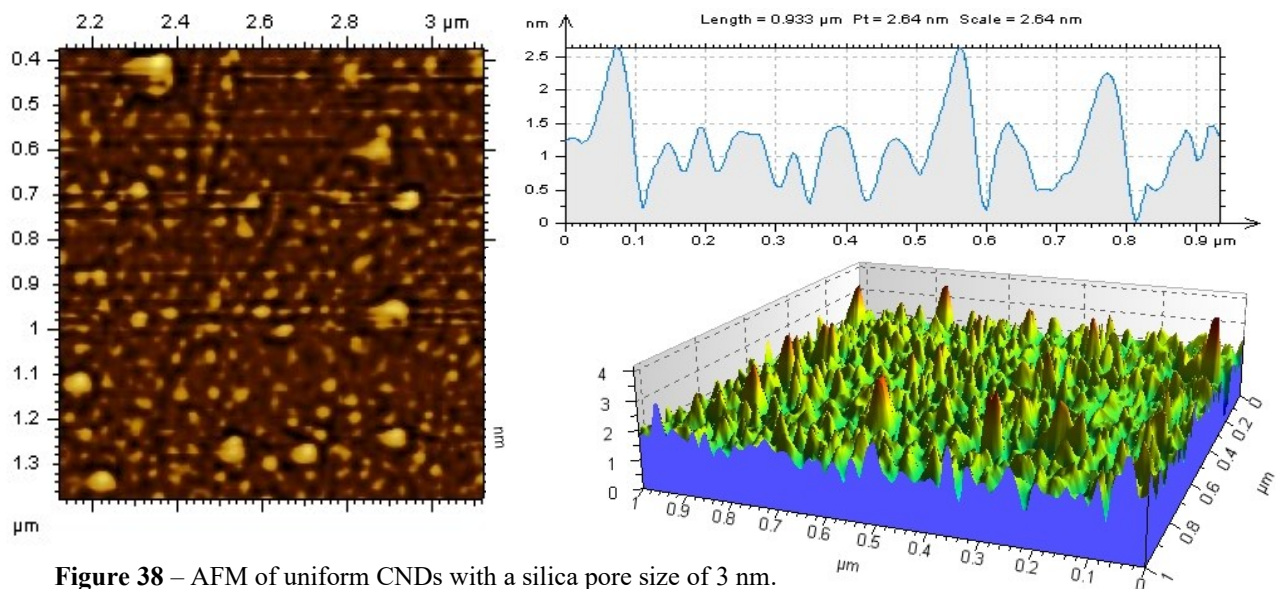


Figure 38 – AFM of uniform CNDs with a silica pore size of 3 nm.

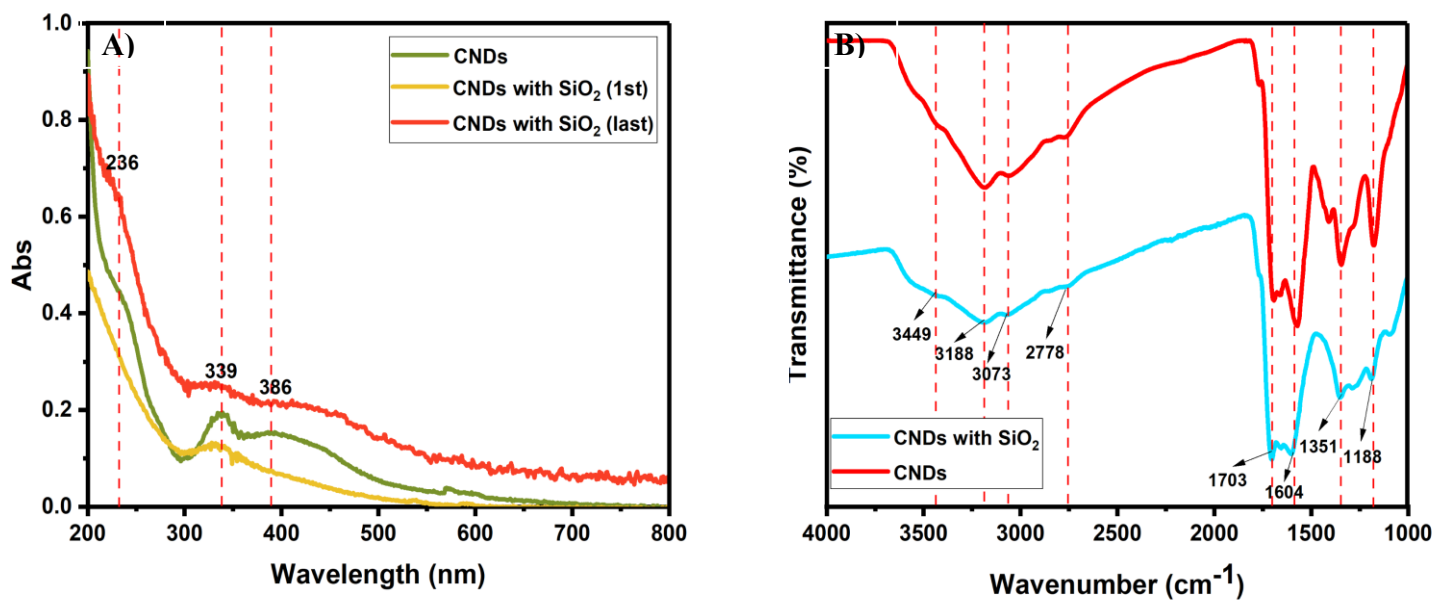


Figure 39 – Comparison between uniform CNDs and CNDs with UV/vis (A) and FTIR (B).

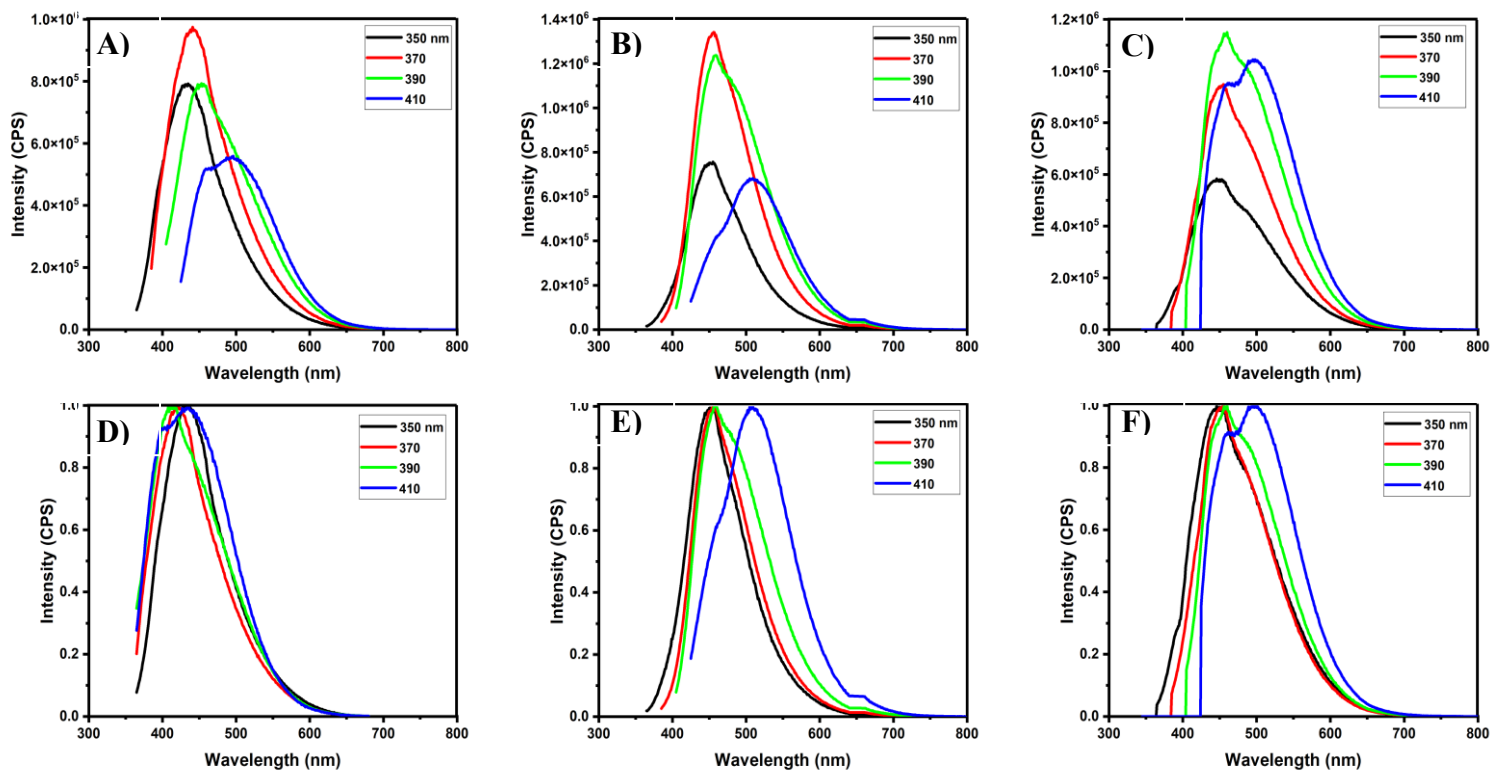


Figure 40 – **A)** PL spectra of CNDs with SiO₂ (1st) – **B)** PL spectra of CNDs – **C)** PL spectra of CNDs with SiO₂ (last) – **D)** Normalized PL spectra of CNDs with SiO₂ (1st) – **E)** Normalized PL spectra of CNDs – **F)** Normalized PL spectra of CNDs with SiO₂ (last).

4. Conclusions

The main goal of this study is to find the most promising kind of carbon dot as CO₂ adsorbent to decrease the amount of CO₂ in the atmosphere considering that, among all the greenhouse gases, it is a main contributor to the climate change. Carbon dots are promising nanomaterials owing to their small particle size, abundant surface functional groups, high surface area and CO₂ selectivity and separation from other gases.

This study was designed by following the order of (1) synthesis of different CDs and their modified counterparts. In order to find the most suitable CD as CO₂ adsorbent, four types of CDs, namely CNDs, G-CDs, P-CDs, and Y-CDs were synthesized by following their own unique well-established procedures; (2) characterizations with UV/vis and adsorption fluorescence emission, Fourier-transform infrared (FTIR) spectroscopies; (3) CO₂ uptake experiments via thermogravimetric analyses to seek the most promising CD species for CO₂ capture; (4) study of the impacts of surrounding moisture and surface functionalities on the CO₂ uptake capacity of CDs. In particular, for G-CDs and P-CDs the ratio of the precursors was changed three times by increasing and decreasing the amount of functional groups such as amine and carboxylic groups in order to understand the correlation between the CO₂ adsorption capacity and the functional groups on the surface of CDs.

As already mentioned, another goal of this study was to reach a uniform-size CNDs in the optic to deepen their structure characteristics related to their properties, analyzed with AFM, FTIR, UV/vis and fluorescence where possible. With a SiO₂ template (pore size of 3 nm) uniform-sized CNDs were obtained with an average size below 4 nm. This approach effectively prevents CNDs inhomogeneity in size while reducing the impact of particle size on various physicochemical properties. Regarding the fluorescence, there were some differences between the regular CNDs and the ones with a silica template: homogeneous CNDs provided a different PL profile that allowed to understand the photoluminescence mechanism of the CDs in general.

By analyzing the TGA of CDs that underwent CO₂ adsorption and desorption processes in their natural state, the CO₂ adsorption capacities of different CD species could be arranged in the order of CNDs and Y-CDs (0.23 mmol/g) < P-CDs (0.64 mmol/g) < G-

CDs (1.52 mmol/g). The high CO₂ adsorption capacity of G-CDs might be associated with the high amine content. This hypothesis was further supported by a high CO₂ adsorption capacity of 3.18 mmol/g of PEHA, an amine-abundant precursor of P-CDs. To investigate the impact of surrounding moisture on the CO₂ uptake capacity of CDs, TGA process was ran on CDs with a dehydration step added prior to CO₂ flush to remove all the water that he could have bound itself to CDs nanoparticles. The insignificant changes in the CO₂ uptake capacities of G-CDs and P-CDs demonstrated the little impact of surrounding moisture on their CO₂ uptake capabilities. Furthermore, TGA was conducted on G-CDs, P-CDs and their modified counterparts and the CO₂ uptake capacities were arranged in the order of G-CDs (1:2) (0.23 mmol/g) < P-CDs (1:2) (0.45 mmol/g) < P-CDs (1:1) (0.53 mmol/g) < and P-CDs (5:1) (0.91 mmol/g) < G-CDs (1:1) (1.4 mmol/g).

A broad range of materials have been investigated for the CO₂ uptake capacity to reduce the level of CO₂ in the atmosphere. And the most inspiring results (already found in the literature reference), with higher CO₂ adsorption capacity than that of CDs, include the GNPs obtained by thermally exfoliating GO sheets in vacuum and with an adsorption capacity of 56.4 mmol/g at 25°C and 30 bar, graphene-Fe₃O₄ with 60 mmol/g at 25 °C and graphene/polyaniline composites with an adsorption capacity of 75 mmol/g, 3.5 times higher than that of pristine graphene (21.6 mmol/g) at 11 bar and 25 °C. In addition, the CO₂ uptake capacities of CDs are comparable to those of amines and functionalized ionic liquids but are lower than those of zeolites and functionalized graphenes.

In summary, CDs have the ability to capture CO₂ and the CO₂ uptake capacity will not be significantly affected by surrounding moisture but can be determined by the content of -OH and/or -NH₂.

Nonetheless, the research on CDs for CO₂ capture is still at its early development stage. The investigation is significant to solve, at least in part, the huge problem of global warming.

Acknowledgements

To my parents, Pia and Pietro, the most important people, for believing in me more than I believed in myself, without whom I would never have reached this milestone.

To Professor Leblanc, an endless thanks for his helpfulness, kindness and humanity that make him a unique professor.

To Professor Tagliaferro, a big thanks for allowing me to do my thesis in the University of Miami and guided me along the path.

To Mattia Bartoli, the best tutor I could have had, an endless thanks for his patience, availability and for teaching me so much.

To my nephews, Carlo, Pietro, Alessandro and Riccardo, as if they were my brothers, to always be here.

To my sisters, Silvia and Serena, that guided me from day 0.

To Cristina, my shoulder, my accomplice and soul mate.

To all my best friends, who have always been a reference for me.

To Giulia, my former roommate as well as best friend with whom fun, support and listening were never missed.

To Arianna and Diego, my homies, who introduced me to Miami and that I miss so much.

To Yiqun, Wei and Braulio, thanks to whom I was able to carry out my project.

To all the international group of my laboratory in the UM, for welcoming me so well, helping me and making me feel at home.

To the Peña-Mendoza family for taking me in like a daughter and never letting me lack anything.

References

- [1] E. Maruccia *et al.*, “Effect of thermal stabilization on pan-derived electrospun carbon nanofibers for co2 capture,” *Polymers (Basel)*., vol. 13, no. 23, 2021, doi: 10.3390/polym13234197.
- [2] E. Maruccia *et al.*, “Nanocast nitrogen-containing ordered mesoporous carbons from glucosamine for selective CO2 capture,” *Mater. Today Sustain.*, vol. 17, p. 100089, 2022, doi: 10.1016/j.mtsust.2021.100089.
- [3] M. L. Liu, B. Bin Chen, C. M. Li, and C. Z. Huang, “Carbon dots: Synthesis, formation mechanism, fluorescence origin and sensing applications,” *Green Chem.*, vol. 21, no. 3, pp. 449–471, 2019, doi: 10.1039/c8gc02736f.
- [4] E. Kirbas Cilingir *et al.*, “Surface modification of carbon nitride dots by nanoarchitectonics for better drug loading and higher cancer selectivity,” *Nanoscale*, vol. 14, no. 27, pp. 9686–9701, 2022, doi: 10.1039/d2nr02063g.
- [5] S. D. Kenarsari *et al.*, “Review of recent advances in carbon dioxide separation and capture,” *RSC Adv.*, vol. 3, no. 45, pp. 22739–22773, 2013, doi: 10.1039/c3ra43965h.
- [6] A. Brunetti, F. Scura, G. Barbieri, and E. Drioli, “Membrane technologies for CO2 separation,” *J. Memb. Sci.*, vol. 359, no. 1–2, pp. 115–125, 2010, doi: 10.1016/j.memsci.2009.11.040.
- [7] R. Balasubramanian and S. Chowdhury, “Recent advances and progress in the development,” *J. Mater. Chem. A Mater. energy Sustain.*, vol. 3, pp. 21968–21989, 2015, doi: 10.1039/C5TA04822B.
- [8] S. Dolai, S. K. Bhunia, S. Rajendran, V. UshaVipinachandran, S. C. Ray, and P. Kluson, “Tunable fluorescent carbon dots: synthesis progress, fluorescence origin, selective and sensitive volatile organic compounds detection,” *Crit. Rev. Solid State Mater. Sci.*, vol. 46, no. 4, pp. 349–370, 2021, doi: 10.1080/10408436.2020.1830750.

- [9] P. Zhu, K. Tan, Q. Chen, J. Xiong, and L. Gao, “Origins of Efficient Multiemission Luminescence in Carbon Dots,” *Chem. Mater.*, vol. 31, no. 13, pp. 4732–4742, 2019, doi: 10.1021/acs.chemmater.9b00870.
- [10] D. M. A. Crista, J. C. G. E. da Silva, and L. P. da Silva, “Evaluation of different bottom-up routes for the fabrication of carbon dots,” *Nanomaterials*, vol. 10, no. 7, pp. 1–15, 2020, doi: 10.3390/nano10071316.
- [11] X. Lin *et al.*, “Carbon dots based on natural resources: Synthesis and applications in sensors,” *Microchem. J.*, vol. 160, no. PA, p. 105604, 2021, doi: 10.1016/j.microc.2020.105604.
- [12] H. peng Feng *et al.*, “Core-shell nanomaterials: Applications in energy storage and conversion,” *Adv. Colloid Interface Sci.*, vol. 267, pp. 26–46, 2019, doi: 10.1016/j.cis.2019.03.001.
- [13] N. A. S. Omar, Y. W. Fen, R. Irmawati, H. S. Hashim, N. S. M. Ramdzan, and N. I. M. Fauzi, “A Review on Carbon Dots: Synthesis, Characterization and Its Application in Optical Sensor for Environmental Monitoring,” *Nanomaterials*, vol. 12, no. 14, 2022, doi: 10.3390/nano12142365.
- [14] E. A. Stepanidenko, E. V. Ushakova, A. V. Fedorov, and A. L. Rogach, “Applications of carbon dots in optoelectronics,” *Nanomaterials*, vol. 11, no. 2, pp. 1–20, 2021, doi: 10.3390/nano11020364.
- [15] G. A. M. Hutton, B. C. M. Martindale, and E. Reisner, “Carbon dots as photosensitisers for solar-driven catalysis,” *Chem. Soc. Rev.*, vol. 46, no. 20, pp. 6111–6123, 2017, doi: 10.1039/c7cs00235a.
- [16] B. Fu *et al.*, “Carbon dots enhanced gelatin/chitosan bio-nanocomposite packaging film for perishable foods,” *Chinese Chem. Lett.*, vol. 33, no. 10, pp. 4577–4582, 2022, doi: 10.1016/j.ccllet.2022.03.048.
- [17] A. Konwar, N. Gogoi, G. Majumdar, and D. Chowdhury, “Green chitosan-carbon dots nanocomposite hydrogel film with superior properties,” *Carbohydr. Polym.*, vol. 115, pp. 238–245, 2015, doi: 10.1016/j.carbpol.2014.08.021.

- [18] Y. Liu and J. Wilcox, “Effects of Surface Heterogeneity on the Adsorption of CO₂ in Microporous Carbons,” *Environ. Sci. Technol.*, vol. 46, no. 3, pp. 1940–1947, Feb. 2012, doi: 10.1021/es204071g.
- [19] Y. Zhou *et al.*, “An insight into embryogenesis interruption by carbon nitride dots: can they be nucleobase analogs?,” *Nanoscale*, 2022, doi: 10.1039/d2nr04778k.
- [20] P. Y. Liyanage *et al.*, “Carbon Nitride Dots: A Selective Bioimaging Nanomaterial,” *Bioconjug. Chem.*, vol. 30, no. 1, pp. 111–123, 2019, doi: 10.1021/acs.bioconjchem.8b00784.
- [21] W. Zhang *et al.*, “Nano-carrier for gene and pentaethylenehexamine modified carbon dots bioimaging based on,” pp. 1–39.
- [22] Y. Zhou *et al.*, “Gel-like carbon dots: A high-performance future photocatalyst,” *J. Colloid Interface Sci.*, vol. 599, pp. 519–532, 2021, doi: 10.1016/j.jcis.2021.04.121.
- [23] Y. Zhou *et al.*, “Gel-like Carbon Dots: Characterization and their Potential Applications,” *ChemPhysChem*, vol. 18, no. 8, pp. 890–897, 2017, doi: 10.1002/cphc.201700038.
- [24] Y. G. Ko, S. S. Shin, and U. S. Choi, “Primary, secondary, and tertiary amines for CO₂ capture: Designing for mesoporous CO₂ adsorbents,” *J. Colloid Interface Sci.*, vol. 361, no. 2, pp. 594–602, 2011, doi: 10.1016/j.jcis.2011.03.045.
- [25] A. I. Pruna, A. Cárcel, A. Benedito, and E. Giménez, “Enhanced CO₂ Capture of Poly(amidoamine)-Modified Graphene Oxide Aerogels with the Addition of Carbon Nanotubes,” *Int. J. Mol. Sci.*, vol. 24, no. 4, 2023, doi: 10.3390/ijms24043865.
- [26] A. Ghosh *et al.*, “Uptake of H₂ and CO₂ by Graphene,” pp. 15704–15707, 2008.
- [27] A. You, M. A. Y. Be, and I. In, “Carbon dioxide adsorption in graphene sheets,” vol. 032152, no. August 2011, pp. 10–16, 2012, doi: 10.1063/1.3638178.
- [28] R. Article, “www.rsc.org/nanoscale,” vol. 6, no. 4, 2014, doi: 10.1039/c3nr04555b.
- [29] D. A. Links, “ChemComm High capacity gas storage in corrugated porous graphene with a specific surface area-lossless tightly stacking manner w,” pp. 6815–6817,

- 2012, doi: 10.1039/c2cc31785k.
- [30] K. Xia, X. Tian, S. Fei, and K. You, “ScienceDirect Hierarchical porous graphene-based carbons prepared by carbon dioxide activation and their gas adsorption properties,” *Int. J. Hydrogen Energy*, vol. 39, no. 21, pp. 11047–11054, 2014, doi: 10.1016/j.ijhydene.2014.05.059.
- [31] E. Environ, “Environmental Science,” pp. 7323–7327, 2012, doi: 10.1039/c2ee21653a.
- [32] D. Zhou, “Graphene – terpyridine complex hybrid porous material for carbon dioxide adsorption,” *Carbon N. Y.*, vol. 66, pp. 592–598, 2013, doi: 10.1016/j.carbon.2013.09.043.
- [33] J. M. Chem, “Nanostructured polyaniline decorated graphene sheets for reversible CO₂,” pp. 3708–3712, 2012, doi: 10.1039/c2jm15385h.
- [34] S. Yang, L. Zhan, X. Xu, and Y. Wang, “Graphene-Based Porous Silica Sheets Impregnated with Polyethyleneimine for Superior CO₂ Capture,” 2013, doi: 10.1002/adma.201204427.
- [35] Z. Sui and B. Han, “Effect of surface chemistry and textural properties on carbon dioxide uptake in hydrothermally reduced graphene oxide,” *Carbon N. Y.*, vol. 82, pp. 590–598, 2014, doi: 10.1016/j.carbon.2014.11.014.
- [36] Y. Zhao, H. Ding, and Q. Zhong, “Applied Surface Science Synthesis and characterization of MOF-aminated graphite oxide composites for CO₂ capture,” *Appl. Surf. Sci.*, vol. 284, pp. 138–144, 2013, doi: 10.1016/j.apsusc.2013.07.068.
- [37] S. Chowdhury, G. K. Parshetti, and R. Balasubramanian, “Post-combustion CO₂ capture using mesoporous TiO₂ / graphene oxide nanocomposites,” *Chem. Eng. J.*, vol. 263, pp. 374–384, 2015, doi: 10.1016/j.cej.2014.11.037.
- [38] W. Huang, X. Zhou, Q. Xia, J. Peng, H. Wang, and Z. Li, “Preparation and Adsorption Performance of GrO @ Cu-BTC for Separation of CO₂ / CH₄,” 2014.
- [39] T. Dasgupta, S. N. Punnathanam, and K. G. Ayappa, “Effect of functional groups on

- separating carbon dioxide from CO₂ / N₂ gas mixtures using edge functionalized graphene nanoribbons,” *Chem. Eng. Sci.*, vol. 121, pp. 279–291, 2015, doi: 10.1016/j.ces.2014.07.057.
- [40] Y. Tian, Y. Lin, T. Hagio, and Y. H. Hu, “Surface-microporous graphene for CO₂ adsorption,” *Catal. Today*, vol. 356, no. June, pp. 514–518, 2020, doi: 10.1016/j.cattod.2020.06.002.
- [41] R. Bera, M. Ansari, S. Mondal, and N. Das, “Selective CO₂ capture and versatile dye adsorption using a microporous polymer with triptycene and 1, 2, 3-triazole motifs,” *Eur. Polym. J.*, vol. 99, no. November 2017, pp. 259–267, 2018, doi: 10.1016/j.eurpolymj.2017.12.029.
- [42] D. G. Boer, J. Langerak, and P. P. Pescarmona, “Zeolites as Selective Adsorbents for CO₂ Separation,” 2023.
- [43] J. Zhao, W. Zhang, D. Shen, H. Zhang, and Z. Wang, “Preparation of porous carbon materials from black liquor lignin and its utilization as CO₂ adsorbents,” vol. 107, no. December 2022, 2023.
- [44] S. Lian, C. Song, Q. Liu, E. Duan, H. Ren, and Y. Kitamura, “Recent advances in ionic liquids-based hybrid processes for CO₂ capture and utilization,” *J. Environ. Sci. (China)*, vol. 99, pp. 281–295, 2021, doi: 10.1016/j.jes.2020.06.034.
- [45] Y. Uehara, D. Karami, and N. Mahinpey, “CO₂ adsorption using amino acid ionic liquid-impregnated mesoporous silica sorbents with different textural properties,” *Microporous Mesoporous Mater.*, vol. 278, no. October 2018, pp. 378–386, 2019, doi: 10.1016/j.micromeso.2019.01.011.
- [46] W. Zhang, E. Gao, Y. Li, M. T. Bernards, Y. He, and Y. Shi, “CO₂ capture with polyamine-based protic ionic liquid functionalized mesoporous silica,” *J. CO₂ Util.*, vol. 34, no. August, pp. 606–615, 2019, doi: 10.1016/j.jcou.2019.08.012.
- [47] F. Nkinahamira, T. Su, Y. Xie, G. Ma, H. Wang, and J. Li, “High pressure adsorption of CO₂ on MCM-41 grafted with quaternary ammonium ionic liquids,” *Chem. Eng. J.*, vol. 326, pp. 831–838, 2017, doi: 10.1016/j.cej.2017.05.173.

- [48] M. M. Wan, H. Y. Zhu, Y. Y. Li, J. Ma, S. Liu, and J. H. Zhu, "Novel CO₂-capture derived from the basic ionic liquids orientated on mesoporous materials," *ACS Appl. Mater. Interfaces*, vol. 6, no. 15, pp. 12947–12955, 2014, doi: 10.1021/am5028814.
- [49] J. Yuan *et al.*, "Amine-functionalized poly(ionic liquid) brushes for carbon dioxide adsorption," *Chem. Eng. J.*, vol. 316, pp. 903–910, 2017, doi: 10.1016/j.cej.2017.02.035.